Nuclear Jacobi and Poincaré transitions at high spins and temperatures: Account of dynamic effects and large-amplitude motion

K. Mazurek,[1,*] J. Dudek,[2,†] A. Maj,[1,‡] and D. Rouvel[2,§]
[1]*Institute of Nuclear Physics PAN, ulica Radzikowskiego 152, Pl-31342 Kraków, Poland*
[2]*IPHC/DRS and Université de Strasbourg, 23 rue du Loess, B.P. 28, F-67037 Strasbourg Cedex 2, France*
(Received 11 February 2013; revised manuscript received 7 January 2015; published 2 March 2015)

We present a theoretical analysis of the competition between the so-called nuclear Jacobi and Poincaré shape transitions as a function of spin at high temperatures. The latter condition implies the method of choice, a realistic version of the nuclear liquid drop model, here the Lublin-Strasbourg drop model. We address specifically the fact that the Jacobi and Poincaré shape transitions are accompanied by the flattening of the total nuclear energy landscape as a function of the relevant deformation parameters, which enforces large-amplitude oscillation modes that need to be taken into account. For that purpose we introduce an approximate form of the collective Schrödinger equation whose solutions are used to calculate the most probable deformations associated with the nuclear Jacobi and Poincaré transitions. We discuss selected aspects of the new description focusing on the critical-spin values for both types of these transitions.

DOI: 10.1103/PhysRevC.91.034301 PACS number(s): 21.60.−n, 21.10.−k, 24.75.+i, 25.70.Gh

I. INTRODUCTION

Atomic nuclei whose properties are governed by strong interactions acting among constituent nucleons can, to an approximation, be considered compact because the volumes of nuclei remain close to the sums of the volumes of these nucleons. This fact, combined with the short range of the nucleon-nucleon interactions and the fact that the nuclear matter can be considered incompressible, makes it possible to introduce a classical notion of nuclear surfaces, at first a paradox because the nucleons *and* nuclei are quantum systems. These surfaces define what is referred to as nuclear shapes.

The notion of generally nonspherical nuclear shapes remains an underlying classical element of quantum mean-field theories of the nucleonic motion in nuclei as described using phenomenological but realistic Woods-Saxon or Yukawa-folded nuclear potentials. These two particular realizations of the nuclear mean field have been used in the past, combined with the so-called Strutinsky method [1]. They were employed to calculate very successfully various nuclear properties such as masses, deformation energies, nuclear moments, angular momenta of excited states, and, more generally, rotational properties together with their evolution with nuclear spin and temperature, to mention just a few elements on the much longer list.

Among important characteristics of atomic nuclei are quadrupole (or higher) charge (and/or mass) moments. Numerous measurements show that the majority of the atomic nuclei are deformed in their ground and excited states and, strictly speaking, among nearly 3000 nuclei so far investigated in the laboratory, only about a dozen may be considered strictly spherical. In fact, these are the nuclei with fully occupied j and/or N shells such as ^{16}O, ^{40,48}Ca, ^{100,132}Sn, or ^{208}Pb and only very few others.

It is well known that an increase of an excitation energy, which within nuclear mean-field theories can be translated into an increase of nuclear temperature, leads to diminishing and possibly to a full disappearance of quantum (shell) effects. Under such conditions, the nuclear energy can be described as a sum of the repulsive Coulomb interactions among the protons together with centrifugal stretching effects associated with the collective rotation and an effective nuclear attraction formally modeled with the help of the concept of the nuclear surface tension. One of the simplest, but at the same time a very successful, modeling of such a physical situation has been achieved within the nuclear liquid drop model, whose ingredients are indeed the competing Coulomb and surface tension mechanisms (cf., e.g., Refs. [2–5]) possibly combined with a collective rotation.

It then follows that the theoretical modeling of the leading features of the motion of macroscopic charged drops, of planets and stars, and of atomic nuclei may, under the discussed conditions, become analogous. The shape evolution which occurs in nuclei may take a form of what is referred to as transitions of Jacobi [6] and Poincaré [7], following suggestions in the above historical articles that such transitions may be induced by rotation of certain astronomical objects. Of course, proposing an analogy between the forms of the behavior of stellar and nuclear objects, as suggested in Ref. [8], may be of a certain aesthetic interest. However, predictions of which critical-spin values and in which nuclei the considered transitions take place constitute a totally different, challenging issue; for early discussions of this issue, cf. Refs. [5] and [9].

The issue of Jacobi and Poincaré shape transitions has received some attention from both the experimental and the modeling viewpoints also more recently as, e.g., in Ref. [10], where a discussion of, among others, Jacobi shape transitions represented with the help of the nuclear effective moments of inertia in the form of "gigantic back bending" can be

*Katarzyna.Mazurek@IFJ.edu.pl
†Jerzy.Dudek@IPHC.CNRS.fr
‡Adam.Maj@IFJ.edu.pl
§David.Rouvel@IPHC.CNRS.fr

found. However, aiming at the use of the Lublin-Strasbourg drop (LSD) approach in the present article, we would like to mention a number of results obtained by combining the LSD analysis with the experimental results of the Cracow-Strasbourg collaboration during the past 10 yr or so.

In this context let us mention, in particular, a successful determination of the presence of the Jacobi transitions in ^{46}Ti reported in Refs. [11,12] together with another one obtained through the observation of the high-energy γ rays and α particles in Ref. [13]. Another interesting result in this mass region was an observation of the preferential feeding of the superdeformed band in cold ^{42}Ca nuclei through the giant dipole resonance γ decay from a very elongated (i.e., possessing a "Jacobi shape") hot rotating ^{46}Ti, followed by the emission of an α particle [14]. A similar problem has been studied in ^{88}Mo; the results can be found in a more recent Ref. [15] (cf. also the studies conducted by other groups such as the ones on the ^{45}Sc [16] and on the ^{47}V nuclei [17].

In all the cases studied a good correspondence between LSD modeling and experiments has been reported. Theoretical predictions for ^{132}Ce based on an extension of the LSD approach to include the modeling of the giant dipole resonance width [18,19] show a good correspondence with measurement as well. Signals of the presence of very large deformations at high spins have been obtained in several nuclei in the mass range $A \sim 120$ in an attempt at combining the search for hyperdeformed nuclear configurations in conjunction with the Jacobi transitions using triple-γ-coincidence measurements [20]. Some preliminary results and discussion concerning the predictions of the Poincaré shape transitions in a few barium nuclei can be found in Refs. [21,22].

Before becoming more precise about the exact subject of the present work, let us recall some earlier efforts in the context of the shape transitions. Early calculations with the liquid drop model suffered from inaccuracies in reproducing the experimental fission barriers; cf. the introduction section in Ref. [9] and references therein. Publications that followed focused first of all on including a description of diffuseness properties of the nuclear surface [23,24], reducing in this way discrepancies between the model and the experimental data. Many publications concerning the nuclear energies on the way to fission discussed first of all the static properties of the nuclear potential energies such as energy positions of the minima and saddle points as a function of both the deformation and the increasing angular momentum. Extensive calculations in Ref. [9], in addition to reviewing the model predictions based on the techniques of those times, addressed, in particular, the issue of the behavior of the nuclear potential in the vicinity of the characteristic (minima, saddle) points by calculating the second-order Taylor expansion around those points and allowing for a local description of the stiffness properties.

In the present article we address first of all the rotation-induced shape transitions in hot rotating nuclei with the help of the liquid drop model in its so-called LSD realization of Refs. [25,26]; cf. also Refs. [27–29]. This approach is combined with that of the collective model, making it possible to go beyond the traditional static description of the nuclear shape changes and calculate, among others, the most probable deformations or the most probable fission-fragment mass asymmetry with the help of the nuclear collective wave functions. Although Jacobi shape transitions have been discussed in the nuclear-physics context by various authors, the Poincaré shape transitions remain largely unknown at present.

The presentation is organized as follows. The next section contains the discussion of the position of our physics problem together with a short description of the macroscopic energy algorithm (LSD) chosen for this article. In Sec. III we derive what appears to us as an efficient algorithm of treating and analyzing the multidimensional deformation spaces in which the total collective nuclear energies will be calculated and possibly competing Jacobi and Poincaré transitions analyzed. At the same time we introduce a short description of the collective model and related Schrödinger equation in curvilinear spaces which will be applied, within approximations, in Sec. VIII. Section IV describes the technical aspects of the extension of the original LSD model with a particular accent on possible inadequacies of the macroscopic modeling of the nuclear neck area. Section V contains the discussion of the technical aspects related to the classical subject of deformation dependence of the fission barriers, whereas Sec. VI is focused on some selected aspects of the spherical-harmonics basis cutoff properties. In Sec. VII we address the issue of the spin dependence of the fission barriers, followed by the discussion of the problem of the large-amplitude motion accompanying the shape transitions of the Jacobi and Poincaré type in Sec. VIII. A summary and conclusions are contained in Sec. IX.

II. PRESENT REALIZATION OF THE LIQUID DROP MODEL

In this article we aim at a *possibly realistic* description of the shape transitions induced by increasing collective rotation in hot nuclei. By the very definition, the shape transitions of interest are those taking place *before the fission limit*, i.e., at spins lower than the critical-spin values for fission, $L < L_{\text{fiss.}}$.

Let us remark in passing that the precise values of the latter reference quantity may be difficult to determine uniquely. What we are interested in, in the present context, are the limiting spin values at which the nuclear system loses totally its stability. In other words, the system's measured lifetimes become too short to be able to prove the presence of such systems in nature so that it makes no sense to dwell upon the associated shape transitions. Within the barrier-penetration model any finite lifetime requires that the corresponding *limiting barrier height is necessarily finite*. Alternatively, one could define $L^{\text{th}}_{\text{fiss.}}$ as the closest integer (half-integer) value at which the calculated fission barrier totally vanishes. As it turns out, a certain arbitrariness in this respect will have no impact on conclusions of the present article, whereas the notion itself will be occasionally convenient in the discussion.

As a matter of convention, in what follows, we apply the term *transition* while speaking about the sequences of shapes as a function of *an increasing* spin; this choice has no impact on the conclusions.

A. Goal's impact on the chosen strategy

One of the goals of this article is to investigate the tools which can be used in studying nuclear symmetry- and symmetry-breaking phenomena within three-dimensional (3D) geometry (the interested reader may consult Ref. [30] for the principles and an overview), in particular at high temperatures. One of the most successful tools capable of producing the results close to the experimental data within the large-scale calculations is the so-called macroscopic-microscopic method of Strutinsky in which the *macroscopic* (read liquid drop model) and the *microscopic* (read phenomenological nuclear mean-field theory) combine to produce a joint scheme. However, it is important to examine by comparing with the experimental results not only both of these tools combined—but when possible—to be able to extract the information on one of them alone. Studying Jacobi and Poincaré shape transitions at high temperatures offers a *unique possibility of controlling—vs experiment—the performance of the macroscopic tool separated from the impact of shell effects* (cf. examples of the studies cited in the previous section, obtained with the use of the LSD model) because of the disappearance of the shell effects at sufficiently high temperatures.

Following this line, in the present article we focus on the macroscopic part alone employing the LSD model with the help of which some rather successful pilot projects [11–21] have been accomplished. In the rest of this section we discuss briefly the arguments related to the precision in the description of the shape-transition aspect. A related, important but a slightly technical aspect of choosing the mathematical approach to study the properties of the nuclear potential in multidimensional spaces is presented in Sec. III in relation to the quantum theory of nuclear collective motion.

Any macroscopic energy expression will be capable of providing the total potential energy maps for predefined spin sequences and thus it will be able to predict a certain evolution of the family of shapes with spin. However, the model which predicts, for instance, fission barriers which are systematically too high (too low) compared with experiment is very likely to provide not only the incorrect/inexact overall shape evolution with spin, but also incorrect critical-spin values at which the competing shape transitions occur, possibly leading to confusion. A possible undesired result would be the prediction of certain shape transitions at spins at which a considered nucleus does not exist anymore because of fission, but other undesired mechanisms can also be envisaged.

In particular, one of those unwanted effects, yet likely to occur, is related to the competition between the Jacobi and Poincaré shape transitions involving shapes of distinct classes and leading, within their respective classes to different types of symmetries below and above the critical transition-spin values, say, $L_{\rm J}^{\rm crit.}$ and $L_{\rm P}^{\rm crit.}$, respectively. The Poincaré transitions lead to the left-right shape asymmetry with predicted asymmetric fission-fragment mass distributions. Should Poincaré transitions *follow* ($L_{\rm J}^{\rm crit.} < L_{\rm P}^{\rm crit.}$) the one of the Jacobi type, the overall elongation of the nuclei undergoing the Jacobi transition will be larger as compared to the opposite case, the corresponding shapes very different, and the predictions of the mass asymmetry drastically influenced. Should the model fail to obtain the right order of the discussed transitions, the model predictions would never be verifiable against the experiment. This would imply a possibly very limited usefulness of the resulting macroscopic description with possibly misleading or erroneous conclusions and conflicting interpretations of the experimental data.

From the above remarks it becomes clear that, through an optimization of the description of the nuclear energies on the way to fission, one may avoid possible undesirable effects just mentioned. In this context there are at least two mechanisms which seem to us obvious to be taken into account. One of them is related to the so-called *congruence-energy effect* introduced and discussed by other authors (for details, cf. the following sections, in which the corresponding mechanism is studied in detail). The other one is related to critical phenomena which accompany the strong shape fluctuations present at the Jacobi- and Poincaré-type shape transitions, a mechanism deserving a special comment, which follows.

Jacobi- and Poincaré-type shape transitions represent not only *just a certain* shape evolution, but first of all, the characteristic symmetry-breaking transformations. In the case of Jacobi transitions as a function of increasing spin, these are the axially symmetric shapes which evolve quickly[1] into a family of triplanar symmetry ones. Similarly, the inversion-invariant ("left-right symmetric") shapes before the Poincaré transitions are replaced by the inversion-breaking shapes after the transition. In what follows it will be practical to introduce symbols $\mathcal{S}_<$ and $\mathcal{S}_>$ to denote the symmetries "before" and "after" one of the two types of the shape transitions. Although it does not necessarily always need to be so, calculations show that the realistic macroscopic energy expressions lead to the significant flattening of the energy landscapes at spins long below the critical-spin values at which the static equilibrium (static energy minimum) shapes change their symmetry: $\mathcal{S}_< \to \mathcal{S}_>$. In several domains of physics these conditions give rise to critical phenomena with strong fluctuations of the related observables, possibly accompanied by the phase transitions, which often require a special attention.

When such a symmetry change occurs, the flatness of the energy landscape implies that it costs very little energy for the nucleus to go from one deformation area to a neighboring one, the corresponding collective wave function varies little, the probabilities remain comparable, and the nucleus undergoes a *large-amplitude vibrational motion*. Under these conditions the *static* shapes, i.e., the ones corresponding to the static energy minimum and the *most probable* deformations, which we refer to as dynamical, may (and often do) differ considerably. So do the theory predictions, e.g., the ones related to nuclear moments and electromagnetic transitions or, possibly, fission-fragment mass distributions and/or other observables, based on the static deformations as compared to the dynamical ones. Because one of our goals is to develop the modeling which, remaining simple, is as realistic as possible,

[1]The phrase "fast evolution" should be understood as a relatively important change in shape at the equilibrium deformation, accompanying relatively small increase in spin, measured, e.g., in steps of $\Delta L = 2\hbar$.

a description of the large-amplitude shape fluctuations during the considered transitions are taken explicitly into account. This will be done by solving the appropriate approximate form of the collective Schrödinger equations, as discussed in Sec. VIII.

B. Comments about the earlier Lublin-Strasbourg drop realization of the model

One of the relatively recent realizations of the liquid drop model, the so-called LSD model (cf. Refs. [25,26]), introduces some extra degrees of freedom associated with the *curvature* of the nuclear surfaces. More precisely, as noticed in the cited references, one may introduce infinitely many geometrically distinct surfaces, which may have the same *surface area* but differ in their forms. They give rise to distinct conditions of the nucleonic motion inside of the considered nuclei and yet, within traditional liquid drop models, they contribute the same surface energy. The surface-curvature term as introduced within the LSD model makes it possible to improve the description of measurable quantities, such as fission barriers and masses, noticeably.

Within a classical modeling of the attractive short-range interactions among particles surrounding a given one inside a nucleus, all their contributions will be mutually compensated, unless we approach the nuclear surface. There, there are no interaction partners *outside* of the delimiting surface, and an uncompensated effective attraction pulling the particles towards the nuclear interior will be created. This attraction will depend on the number of considered particles per unit volume, which, in turn, will be different for, e.g., locally concave vs locally convex surface areas; hence the need to introduce the surface-curvature considerations. It then follows that for any varying surface with the fixed surface area, the nuclear surface-energy contributions will be constant, whereas the curvature contribution will vary depending on the variation of the local curvature.

Using the concept of the curvature of the nuclear surface, the parameters of the LSD model have been adjusted to the nuclear masses in Ref. [25], and, as it turned out, the description of nuclear fission barriers has been considerably improved with respect to the best-performing preceding versions of the liquid drop model. This has been achieved without introducing any fit conditions related to the experimental barrier heights. Such an improvement can be considered as a demonstration of an intrinsic, physical consistency of the LSD model which contains one more (and known in classical physics) effective-interaction mechanism, the surface curvature.

An improved description of certain nuclear properties ultimately encourages an exploration of this new version of the liquid drop model to describe nuclear mechanisms which, so far, were considered to correspond to a higher level of sensitivity. Our choice here is to investigate the rotation-induced shape transitions, whose critical spins depend in a sensitive way on the details of the energy expression.

The macroscopic nuclear liquid drop model energy in its LSD form can be expressed using a number of terms representing the nuclear energy as a function of the proton and the neutron numbers, Z and N, respectively, as well as the nuclear deformation in the form

$$\begin{aligned} &E_{\text{total}}(N,Z;\alpha;L) \\ &\quad = E(N,Z) + E_{\text{Coul.}}(N,Z;\alpha) + E_{\text{surf.}}(N,Z;\alpha) \\ &\qquad + E_{\text{curv.}}(N,Z;\alpha) + E_{\text{rotat.}}(N,Z;\alpha;L), \end{aligned} \tag{1}$$

where L denotes the nuclear collective angular momentum and α represents the ensemble of all the deformation parameters used. In the above expression, we find the deformation-dependent electrostatic Coulomb, $E_{\text{Coul.}}(N,Z;\alpha)$, the surface, $E_{\text{surf.}}(N,Z;\alpha)$, and the curvature, $E_{\text{curv.}}(N,Z;\alpha)$, energy terms (the latter characteristic of the LSD realization of the model) and the rotational energy, $E_{\text{rotat.}}(N,Z;\alpha;L)$, respectively. The first term on the right-hand side in Eq. (1) denotes by definition the combined, deformation-independent terms, possibly including the original, deformation-independent version of the so-called congruence-energy expression; see below.

The above expression can be standardized to represent the atomic mass. In such a case the deformation-independent term is given by (for a complete atomic mass formula used here; cf. also Ref. [25] and references therein)

$$\begin{aligned} E(N,Z) &= ZM_{\text{H}} + NM_{\text{n}} + E_{\text{elect.}}(Z) \\ &\quad + E_{\text{vol.}}(N,Z) + E_{\text{cong.}}(N,Z), \end{aligned} \tag{2}$$

where $E_{\text{elect.}}(Z) = -b_{\text{elect.}}Z^{\epsilon}$, with $\epsilon = 2.39$ and with $b_{\text{elect.}} = 1.433 \times 10^{-5}$ MeV. The latter term parametrizes the binding energy of the electrons, whereas the other two terms represent Z masses of the hydrogen atom and N masses of the neutron, respectively. The deformation-independent congruence-energy term, as used in the literature in the past, is replaced with a deformation-dependent one; cf. Eq. (9) and the surrounding text.

The volume energy in Eq. (2) is parametrized as

$$E_{\text{vol.}}(Z,N) = b_{\text{vol.}}(1 - \kappa_{\text{vol.}}I^2)A, \tag{3}$$

where $I = (N-Z)/(N+Z)$. [All the parameters appearing implicitly in Eq. (1), such as $b_{\text{vol.}}$ and $\kappa_{\text{vol.}}$ and the ones which appear below, are collected in Table I.]

The Coulomb liquid drop model (LDM) term in its "traditional form" reads

$$E_{\text{Coul.}}(N,Z;\alpha) = \frac{3}{5}e^2\frac{Z^2}{r_0^{\text{ch}}A^{1/3}}B_{\text{Coul.}}(\alpha) - C_4\frac{Z^2}{A}, \tag{4}$$

TABLE I. The parameters of the LSD model fitted to the measured atomic masses only, i.e., without using the information about the fission barriers (from Ref. [25]).

Term	Units	LSD
$b_{\text{vol.}}$	MeV	−15.4920
$\kappa_{\text{vol.}}$	1	1.8601
$b_{\text{surf.}}$	MeV	16.9707
$\kappa_{\text{surf.}}$	1	2.2938
$b_{\text{curv.}}$	MeV	3.8602
$\kappa_{\text{curv.}}$	1	−2.3764
r_0^{ch}	fm	1.21725
C_4	MeV	0.9181

with the mass number $A = Z + N$, the electric charge unit denoted e, and the so-called charge radius parameter $r_0^{\rm ch}$. The term proportional to Z^2/A represents the nuclear charge-density diffuseness correction, whereas the deformation-dependent term, $B_{\rm Coul.}(\alpha)$, denotes the Coulomb energy of a deformed nucleus normalized to that of the sphere with the same volume.

The surface energy in its "traditional" LDM form reads

$$E_{\rm surf.}(N,Z;\alpha) = b_{\rm surf.}(1-\kappa_{\rm surf.}I^2)A^{2/3}B_{\rm surf.}(\alpha). \quad (5)$$

Here the deformation-dependent term, $B_{\rm surf.}(\alpha)$, is defined as the surface energy of a deformed nucleus normalized to that of the sphere of the same volume.

The curvature term is given by

$$E_{\rm curv.}(N,Z;\alpha) = b_{\rm curv.}(1-\kappa_{\rm curv.}I^2)A^{1/3}B_{\rm curv.}(\alpha), \quad (6)$$

with

$$B_{\rm curv.}(\alpha) = \int_0^{\pi} d\vartheta \int_0^{2\pi} d\varphi \left[\frac{1}{R_1(\vartheta,\varphi;\alpha)} + \frac{1}{R_2(\vartheta,\varphi;\alpha)}\right], \quad (7)$$

where R_1 and R_2 are deformation-dependent principal radii of the nuclear surface at the point position defined by spherical angles ϑ and φ.

The parameters entering all the above expressions are given in Table I.

These parameters are kept without modification in the present article, whereas the deformation-dependent congruence-energy term introduces a new parametric freedom as discussed in the following section.

Finally, the rotation-energy term is defined, as usual, by

$$E_{\rm rotat.}(Z,N;\alpha;L) = \frac{\hbar^2}{2\mathcal{J}(Z,N;\alpha;L)}L(L+1), \quad (8)$$

with the classical moment of inertia $\mathcal{J}$ calculated at the given deformation α. In the following applications we assume, without losing generality, that rotation takes place about the $\mathcal{O}_y$ axis (for more details, see below).

C. Comments about the precision of the numerical integration at the extreme elongations

The numerical realization of the algorithm calculating the geometrical factors in Eqs. (4)–(6), i.e., $B_{\rm Coul.}$, on the one hand and $B_{\rm surf.}$ and $B_{\rm curv.}$ on the other, involves the fourfold and the twofold integrations, respectively. The corresponding integrals over the spherical angles $0 \leqslant \vartheta \leqslant \pi$ and $0 \leqslant \varphi \leqslant 2\pi$ (in the case of the double integrals and, additionally, over $0 \leqslant \vartheta' \leqslant \pi$ and $0 \leqslant \varphi' \leqslant 2\pi$ in the case of the fourfold ones) are performed using the standard Gauss-Legendre quadrature expressions.

Among the three integrals needed, the Coulomb term is usually considered the most demanding because it involves, in principle, the sixfold integration. One can demonstrate that with the help of the double application of the Gauss-Ostrogradsky theorem the corresponding integrals can be transformed to a double surface-integration form (cf., e.g., Ref. [31]), and this approach has been used here.

TABLE II. Convergence properties of the double integrals needed to calculate the surface- and curvature-energy terms, for increasing number of the Gaussian order parameters N_ϑ. We have selected an axial-symmetry shape that resembles two touching ellipsoids with $\alpha_{20} = 3.0, \alpha_{40} = 0.2$; in the case of the axial symmetry, the integration does not depend on φ.

N_ϑ	$B_{\rm surf.}$	$B_{\rm curv.}$
34	1.280 102	1.584 938
50	1.280 036	1.574 277
66	1.280 017	1.567 360
82	1.280 010	1.563 163
98	1.280 008	1.560 719
112	1.280 007	1.559 463
128	1.280 006	1.558 625

To assure the requested precision without unnecessary losses of the CPU time the performance of the integrations can be optimized by adjusting appropriately the orders of the Gauss quadratures N_ϑ, N_φ, $N_{\vartheta'}$, and $N_{\varphi'}$ for each integration separately, taking into account the specificity of the integrands and the physicist's needs as far as the level of precision is concerned. In particular, the identical Gauss orders for the integrations over ϑ and ϑ' as well as φ and φ' should be avoided for the Coulomb energy related integration, because of the singularities of the $\sim|\vec{r}-\vec{r}\,'|^{-1}$ term in the Coulomb integral.

The techniques in question are quite standard by now and have been in frequent use for some time in the present or similar contexts; cf. Ref. [32] and, in particular, Refs. [33,34]. Because, however, the illustrations of the stability issue for the typical integrals needed for the macroscopic nuclear energy have not been published, a few illustrative aspects will be presented in Tables II–V.

In Table II we illustrate the convergence properties of $B_{\rm surf.}$ and $B_{\rm curv.}$ as functions of the increasing numbers of the Gauss-integration nodes at the deformation point chosen in such a way that the corresponding shape is very close to the form of

TABLE III. Similar to the results in the preceding table at an exotic shape with exotic nonaxialities. The shape is defined by $\alpha_{20} = 2.0$, $\alpha_{22} = 0.8$, $\alpha_{40} = 0.8$, $\alpha_{44} = 0.4$, $\alpha_{66} = 0.2$, and $\alpha_{88} = 0.1$. The combination of α_{20} and α_{22} above implies the quadrupole triaxiality of $\gamma \approx 30^\circ$. We have fixed the number of nodes for the Gauss integration over ϑ at $N_\vartheta = 128$, the last value tested for the axial configuration in Table II.

N_φ	$B_{\rm surf.}$	$B_{\rm curv.}$
34	1.420 029 36	1.480 921 42
64	1.420 026 80	1.481 236 47
88	1.420 026 46	1.480 984 81
112	1.420 026 47	1.480 998 87
136	1.420 026 47	1.481 001 63
160	1.420 026 47	1.481 000 48
180	1.420 026 47	1.481 000 69
200	1.420 026 47	1.481 000 73

TABLE IV. Convergence properties of the Coulomb energy terms. Here we have selected a deformation point characteristic of two separating ellipsoids as in Table II. Because of the axial symmetry the results depend on N_ϑ and $N_{\vartheta'}$. For the Coulomb energy, a very good stabilization is obtained at the level of 50–70 Gauss-integration points.

N_ϑ	$N_{\vartheta'}$	$B_{\mathrm{Coul.}}$
18	28	0.834 097 34
26	36	0.834 098 13
34	44	0.834 098 02
42	52	0.834 098 14
50	60	0.834 098 14
58	68	0.834 098 14

two touching ellipsoids. This is a particularly demanding test for the curvature-dependent term. The results in Table II show that the stability of the integration is achieved for sufficiently (although not extremely) large number of integration points.[2]

Results of a similar test but for a strongly nonaxial shape are presented in Table III at the less extreme elongation of $\alpha_{20} = 2$, yet with a pretty well formed neck. To stabilize the integration result at the level $\approx 10^{-6}$, one would need twice as many integration points as in the case of the Coulomb energy (cf. Tables IV and V).

A similar test but for the Coulomb energy term which involves generally the fourfold integration, is illustrated in Tables IV and V. As before, the selection of the numbers of the Gauss-integration nodes for the four variables is, to an extent, arbitrary and should guarantee acceptable accuracy at the possibly small number of integration points. The illustrations give certain indications about the precision cost in terms of the node numbers.

[2]The length of the integration interval for the second variable, φ, is double the one for the fist variable, ϑ, and one may be tempted to nearly double the number of Gauss-integration points for the former one. However, the specificity of the parametrization used here is such that the nuclear elongation and neck formation (convex vs concave forms) are mainly "taken care of" by the dependence on ϑ, whereas the nonaxiality effects that usually do not involve concave surfaces are mainly described by φ. One can use this property to optimize N_φ at less than $2N_\vartheta$.

TABLE V. Convergence properties of the explicitly fourfold integrals when calculating the Coulomb energy contribution for increasing number of the Gaussian node numbers N_ϑ and N_φ as well as $N_{\vartheta'}$ and $N_{\varphi'}$. Here we use the same deformation point as in Table III with an exotic nonaxiality. A very good stabilization is obtained at the level of 50–70 Gauss-integration points.

N_ϑ	N_φ	$N_{\vartheta'}$	$N_{\varphi'}$	$B_{\mathrm{Coul.}}$
18	26	28	34	0.820 430 84
26	34	36	42	0.820 453 68
34	42	44	50	0.820 470 42
42	50	52	58	0.820 470 64
50	58	60	66	0.820 470 63
58	66	68	74	0.820 470 66

D. Comments about the deformation-dependent congruence-energy term and critical spins

The congruence-energy contribution to the nuclear LDM was originally introduced in a purely phenomenological manner in Ref. [4], without taking into account its possible deformation dependence. It was modified next by introducing a multiplicative shape-dependent factor [35,36], aiming at the improvement of the description of the fission process and, in particular, the transformation of an original parent nucleus into two separated fission fragments. The shape-dependent factor in Ref. [35] was defined in terms of the ratio between the radius of the neck and the mean value of the radii of the nascent fragments [cf. Eqs. (5) and (7) in the quoted reference], whereas in Ref. [37] it was defined in terms of the cross sections through the neck and the maximum cross section through the smallest nascent fragment.

The phenomenological definitions are usually based on the intuition that for geometrically compact shapes, i.e., relatively far from the neck formation, the congruence energy should not be sensitive to small deformation changes. On the contrary, this factor is expected to have an increasing impact on the total nuclear energy, caused by the congruence mechanism for the more and more necked-in shapes. It should be emphasized at this point that the intuitive argumentation quoted can by no means be treated as a replacement for a better founded microscopic one (which, however, to our knowledge, does not exist in the literature so far).

The arguments in favor of introducing the deformation dependence in the congruence-energy term bring us to the necessity of a modification of the structure of the original LSD expression in Eq. (1), in that

$$E(N,Z) \rightarrow E_0(N,Z) + E_{\mathrm{cong.}}(N,Z;\alpha), \tag{9}$$

where the new deformation-independent term becomes $E_0(N,Z) = ZM_{\mathrm{H}} + NM_{\mathrm{n}} - 0.000\,014\,33\,Z^{2.39} + E_{\mathrm{vol.}}$. The modified, deformation-dependent congruence-energy contribution is denoted $E_{\mathrm{cong.}}(N,Z;\alpha)$ from now on.

To optimize the description of the observables that can be tested experimentally, we need, among others things, to determine the critical spin values corresponding to the onset of the triaxial (Jacobi) and the left-right asymmetry (Poincaré) shape transitions. Introducing the deformation-dependent congruence-energy term plays an important role in improving the description, especially for certain mass regions (cf. Sec. IV). This information is used in conjunction with the quantum description of large-amplitude shape fluctuations driven by the flattening of the nuclear energy surfaces accompanying such transitions, Sec. VIII.

Analogous considerations which explicitly include thermal shape fluctuations, describe rather satisfactorily the strength function of the giant dipole resonance (GDR). The latter have been excited and successfully analyzed [12] in a few hot rotating compound nuclei to study the Jacobi shape transition. This encourages the extension of this type of technique to a

more systematic analysis of various nuclear shape fluctuations after improving further the performance of the LSD approach.

In the following sections we illustrate and discuss our present realization of the LSD model in which we include a deformation-dependent congruence-energy contribution in an attempt to improve further the description of the experimental data on fission barriers. This leads to an extension of the range of applicability of the macroscopic model at hand to a more refined level of precision. In such a way we could better approach a delicate balance between Jacobi and Poincaré shape transitions at high spins especially in the presence of the dynamical effects accompanying the large-amplitude oscillations and, moreover, introduce a simplified, approximate description of these dynamical effects when discussing the nuclear behavior at scission.

III. COLLECTIVE MOTION AND POTENTIAL-ENERGY HYPERSURFACES IN MULTIDIMENSIONAL SPACES

We wish to emphasize that employing the potential-energy surfaces in the description of the nuclear collective motion—to provide theory predictions comparable to experiment—is ultimately related to the problem of the deformation-dependent collective inertia. Indeed, the role of the inertia tensor briefly summarized in this section represents the *sine qua non* condition for the theoretical estimates of, e.g., fission lifetimes as well as those of the shape isomers—but, of course, practically of all the observables associated with the collective motion, such as transitions and their probabilities—within microscopic theories.

The role of the collective inertia tensor is at the same time one of the most difficult elements for the direct comparison with experiment. This is because such comparison can only be performed at a certain significance level after solving the collective Schrödinger equation [Eq. (13) in Sec. III A] in the spaces of sufficiently rich dimensionality and for sufficiently many nuclei. This is a very complex and challenging task which, to our knowledge, has not been achieved yet, except for some selected and rather limited situations.

One of the important consequences of the quantum and dynamical nature of the nuclear collective problem is that many *apparently important details* of the potential hypersurfaces, as well as certain variations of the inertia tensor (the latter present only at the low-temperature limit), are "smeared out" when the solutions of the Schrödinger equation in the multidimensional spaces are sought. This is because the corresponding solutions are obtained after diagonalizing the Hamiltonian matrix composed of the integrals in which, e.g., certain types of fluctuations in the integrand are mutually compensated and play no explicit role anymore. As a consequence, the information about the "very, very exact" numerical properties of the local minima and the saddle points is usually lost on the way to the final result expressed in terms of probabilities or the collective wave functions which depend on the integrals in question. The precise analysis of the numerical values characterizing the saddle points is a nontrivial problem as stated by other authors and briefly discussed below. This information (without discouraging as precise as possible a numerical calculation) may allow for a certain flexibility in seeking an optimum between numerical rigor and the computer CPU time, a message particularly worth considering in the case of the large-scale calculations.

A. Guidelines implied by quantum theory of collective motion

Let us briefly summarize the general framework of the quantum theory of the collective nuclear motion. For this purpose we briefly reintroduce the principal notions such as the deformation-dependent mass tensor or curvilinear spaces of collective variables. This will place the issue of the potential-energy hypersurfaces at a perspective of one among several factors which combine together in the quantum description of the collective effects. Even though, for the mathematical simplicity reasons, we do not use the microscopically calculated mass tensor in this particular article (such project is in progress and the results will be published elsewhere), we wish to recall a few underlying properties. This part of the discussion at the same time serves as an introduction to the treatment of the large-amplitude motion which in this article is based on an approximate version of the general formalism (cf. Sec. VIII for illustrations).

The number of nuclear collective variables necessary to describe the shape effects realistically needs to be larger than two, which implies that the easy analyses that can immediately be tested using two-dimensional contour plots will not be directly applicable. Mathematically, our problem consists of calculating, analyzing, and interpreting the behavior of a scalar function, say V (the nuclear potential energy), of a vector argument built out of contravariant tensor components $\{\alpha^1,\alpha^2,\ldots,\alpha^n\} \equiv \alpha$, as well as a symmetric $n \times n$, covariant inertia tensor, $B_{ij}(\alpha)$, in an n-dimensional vector subspace of collective coordinates. [In our case these collective spaces (subspaces) are spanned by the spherical tensors $\alpha^{\lambda\mu}$ playing the role of the expansion coefficients in terms of the spherical harmonics; cf. Eq. (14) below.]

As is well known, *in principle*, the description of the nuclear motion with the help of the nuclear surface is a fully quantum process described within the collective Hamiltonian, the collective model of Bohr being one of the best known examples. In such an approach one begins with the concept of the inertia tensor entering a classical (to start with) kinetic energy expression,

$$T_{\text{class.}} = \frac{1}{2}\sum_{i,j} B_{ij}^{\text{class.}}(\alpha)\dot{\alpha}^i\,\dot{\alpha}^j, \tag{10}$$

where the symbols $\{\alpha^i\}$ represent the contravariant realization of the collective coordinates defining the equation of the nuclear surface (for details cf., e.g., Ref. [38]). The inertia tensor must appear here in its covariant form, in which case it is expressed in the units of MeV s^2.

The mass tensor whose components are used to write the Schrödinger equation of the collective nuclear motion are usually calculated microscopically, employing rather advanced methods of the perturbation theory. In relation to, for instance, the usual phenomenological mean-field Hamiltonians such as those based on the deformed Woods-Saxon or Yukawa-folded potentials, the corresponding formulas can be obtained

explicitly following the proposition in Ref. [39], though the calculations must be performed numerically. (An extended discussion of this problem can be found in Ref. [38], whereas for an alternative approach applying the generator coordinate method in the description of the nuclear inertia, the reader is referred, e.g., to Ref. [40].)

The quantum version of the Hamiltonian with the classical kinetic energy as in Eq. (10) is obtained using the standard by now, a quantization procedure; cf. Refs. [41,42]. The collective Schrödinger equation, whose an approximate version is solved below in Sec. VIII, is obtained with the Hamiltonian whose form, after Schrödinger's original article about his quantization,[3] reads

$$\hat{H}_{\text{quant.}} = \frac{-\hbar^2}{2\sqrt{B}} \sum_{i,j=1}^{n} \frac{\partial}{\partial \alpha^i}(\sqrt{B} B^{ij}) \frac{\partial}{\partial \alpha^j} + V. \qquad (11)$$

Here $B \equiv |\det[B_{ij}]|$ is the absolute value of the determinant of the covariant representation of the mass tensor, whereas V is the collective nuclear potential, e.g., the one calculated using the Strutinsky method or, as in our case, the LDM. [Recall that $\sum_j B_{ij} B^{jk} = \delta_i^k$ and, consequently, the units of the components of the contravariant representation of the inertia tensor are reciprocal to those of the covariant representation. The units of the covariant components are $[B_{ij}] = \text{MeV s}^2$; however, in the case of the applications in the context of the Schrödinger equation in the curvilinear spaces one often finds in the literature $[B_{ij}] = \hbar^2\ \text{MeV}^{-1}$. The units of the determinant factor are $[|\det B|] = \text{MeV}^n\ \text{s}^{2n}$ so that the generalized kinetic energy in Eq. (11) is expressed, as expected, in MeV.]

The tensor of inertia enters not only on the level of the equations of the motion with the Hamiltonian in Eq. (11), but very importantly through a "reinterpretation" of the probability of finding the system in the curvilinear space. The latter probability is given by

$$dP_N(\alpha) = \Psi_N^*(\alpha)\Psi_N(\alpha)\sqrt{B(\alpha)}\, d\alpha, \qquad (12)$$

where Ψ_N are the solutions of the collective Schrödinger equation,

$$\hat{H}_{\text{quant.}}\Psi_N = E_N \Psi_N. \qquad (13)$$

Very importantly, in multidimensional spaces it is then sufficient that a few components of the inertia tensor increase in a certain range of the deformation space and the determinant factor in Eq. (12) grows very quickly as a function of the *products* of various components of the tensor. This mechanism may turn out being occasionally very important in that the calculated maximum probabilities, strictly speaking, follow neither the stationary points on the potential hypersurfaces nor the steepest descent valleys. How importantly the probability expression in Eq. (12) may change the simplified interpretations based on the static potential-energy hypersurfaces can be seen, e.g., from the illustrations in Figs. 1–3 in Ref. [43].

[3]There exist several alternative, equivalent forms of the Laplacian expression written in the Riemannian (curvilinear) spaces. Here we use the one which is the simplest formally; cf. Ref. [42].

The collective model schematized above has been applied rather rigorously in the description of the leading quadrupole nuclear collective motion by several authors; the reader is referred to the review in Ref. [44]. This is a rather exceptional, and indeed rare, case in the present context, where the principles of the quantum and microscopic theories are followed down to the final solutions including the calculations of the electromagnetic transition probabilities.

In contrast, in the applications to the large-amplitude motion, as for example in the case of nuclear fission, extra simplifying assumptions have been often employed. They consist in combining the 1D approximation with the path integral and the Ritz-Rayley methods (cf., e.g., Ref. [45]) or in using, typically, 2D projections to avoid working with the full n-dimensional space. The idea of considering probabilities for passing through a given area of the deformation space surrounding, e.g., a static minimum point to another area surrounding another static characteristic point (e.g., another minimum, saddle or scission points) along a single path has been implicitly criticized;[4] cf., e.g., Ref. [46]. Indeed, the authors of the cited article stress the importance of yet another mechanism that takes the form of "dynamical corrections," those originating from the mechanism of the zero-point motion.

We can summarize this part of the discussion in the following way.

(i) The description of the nuclear quantum systems, especially in the regime of the large-amplitude motion, should employ a quantum formalism such as, e.g., one of the realizations of the collective model.

(ii) The corresponding description of the motion should take into account the dynamical effects modeled with the help of the inertia tensor, at the expense of a considerable complication of both the formalism and the complexity of the computing algorithm.

(iii) The nuclear potential energy calculated, e.g., with the help of either Hartree-Fock or Strutinsky methods, or, alternatively, with the help of the classical parametrization using macroscopic models (LDM, LSD, etc.), plays the role of the *quantum potential* in the collective Schrödinger equation [cf. Eq. (13)].

(iv) Static approaches can be considered as certain approximations to the quantum-collective description. In this sense, drawing the experiment-comparable conclusions about the nuclear quantum systems out of static energy landscapes alone can be seen as an approximation to the collective-model description.

[4]More precisely, because the deformation space is composed of an infinite number of densely distributed points and because the probability of reaching any point of null measure is null, in strictly mathematical terms the probability of passing through any preselected point is zero. Accordingly, the physical significance is rather attributed to the probabilities in the form of $dP_N(\alpha)$ of Eq. (12), as well as some derived integral forms, and/or the appropriate weighted averages in the quantum formalism of collective model.

This being said, the collective model is again a certain convenient *approximation* to the description of the nuclear many-body problem. In the present article, we address the question of the shape transitions using potential energies calculated with the macroscopic model and solving an approximate version of the collective nuclear Schrödinger (thus quantum) equation; see Sec. VIII.

B. Guidelines implied by the multidimensional character of the collective motion

The starting point in the construction of macroscopic (and macroscopic-microscopic) nuclear models consists of defining the underlying class of geometrical surfaces describing the nuclear shapes and of parametrizing these shapes with the collective coordinates within a "reasonable" subset of $\mathbb{R}^n$. One of the strategies found in the literature relies on focusing on a very limited number of parameters while preserving the necessary minimum of "really needed" degrees of freedom. For instance, parametrizations employing two spheroids, either overlapping or smoothly joined, were in use as, e.g., the ones joined by another spheroid or a hyperboloid to choose between necked-in and already separated systems [47]. A discussion of the latter and some alternative, few-parameter, choices can be found in Ref. [37]. Some other choices involve the nuclear elongation, triaxiality, and left-right asymmetry.

The issue of the parametrization of the nuclear shape is closely related with the mathematical implications on the level of determining the characteristic points of physical interest, such as saddle points or local minimum points in multidimensional spaces. This problem is not trivial and far from being solved. In particular, as pointed out in the recent Ref. [48], which discusses the uncertainties related to the saddle points in multidimensional spaces

(i) every point that appears as stationary (e.g., minimum) on the energy surface in an n-dimensional space *will, in general, not be stationary* in the m-dimensional space for $m > n$;
(ii) every point that appears as a saddle in an n-dimensional space *will, in general, not be a saddle point* in the m-dimensional space with $m > n$.

The latter item has natural implications for the present project: Because we wish to study a possible coexistence between the shape transitions of two competing distinct symmetries; for this type of the project it will be of advantage to keep a certain flexibility in terms of the dimensions of the deformation space. In other words, we will consider a shape representation in terms of an n-dimensional subset of the (in principle infinite) basis set of functions, with n playing a role of the control, basis cutoff parameter. This will make it possible to test the reactions of the model with respect to varying hypotheses concerning the symmetry and/or the number of the basis elements. In particular, the axial and nonaxial shapes will enter the tests simultaneously (and flexibly with the possibility of increasing or decreasing the number of basis functions) to be able to treat the Jacobi and Poincaré shape transitions on the same footing.

C. The issue of shape parameterization and minimization scheme in multipole space $\{\alpha_{\lambda\mu}\}$

In the present realization of the LSD model we wish to make the results of the calculations possibly independent of the limitations mentioned. This can be done at the expense of the time of the numerical calculations, and the only way to achieve such a goal is to expand the nuclear surface in terms of a *basis set of functions* such as spherical harmonics $\{Y_{\lambda\mu}\}$. The latter have been used for a long time in the present context (e.g., Refs. [49–51]),

$$R(\vartheta,\varphi) = R_0 c(\alpha)\left[1 + \sum_{\lambda=2}^{\lambda_{\max}} \sum_{\mu=-\lambda}^{\lambda} \alpha^{\lambda\mu} Y_{\lambda\mu}(\vartheta,\varphi)\right], \qquad (14)$$

where $\alpha \equiv \{\alpha^{\lambda\mu}\}$ and where function $c(\alpha)$ is obtained from the nuclear volume conservation condition. (Let us mention in passing that the contravariant tensor $\alpha^{\lambda\mu}$ is proportional to $\alpha^*_{\lambda\mu}$ and that the two can be identified with the help of an appropriate choice of the phase conventions.)

The maximum multipolarity used, $\lambda_{\max}$, plays the role of the basis cutoff parameter and replaces the generic symbol for the space dimension, n, used so far. It is an advantage of such an approach that by increasing the cutoff we can test and decide about achieving (or not) the stability of the final result with respect to the selected set of the basis functions under the user-chosen stability criteria; cf. Secs. IV–VI.

Let us remark at this point that an axially symmetric analog of the expansion in terms of the spherical-harmonic basis has been used in Ref. [52] with the Legendre-polynomial expansion, which can be considered as a particular case of the spherical-harmonics series. However, in contrast to Eq. (14), in which certain exotic forms cannot be obtained, when the point position on the nuclear surface cannot be expressed as a unique function of ϑ and φ, in the quoted reference the expansion variable used was the distance from the nuclear axis to the nuclear surface, thus allowing for a description of shapes going beyond the binary-fission configurations (with, e.g., a possibility of parameterizing three- or four-fragment configurations). An extension of the discussed choice has been introduced in Ref. [9], making it possible to consider the triplanar forms with the possibility of parameterizing simultaneously the multineck configurations.

The present parametrization in terms of spherical harmonics does not include such possibilities. Instead, it offers a series of advantages in certain nuclear structure theory developments that go beyond the pure macroscopic model aspects. For instance, in the regime of low or, at the extreme limit, zero temperatures, one is interested in the strongest shell effects whose research is largely facilitated by combining the mean-field and the point-group theory techniques, the latter using preferentially the spherical harmonics representation (the interested reader is referred to Refs. [30,53] and references therein). Another important context in which the use of spherical harmonics largely facilitates the modeling concerns the uniqueness of the transformation between the intrinsic and laboratory reference frame (the so-called problem of the symmetrization group) when calculating electromagnetic

transition probabilities out of the solutions of the collective-model Hamiltonian; cf. Ref. [54].

Minimization of a scalar function depending on vector arguments is a task whose complexity increases with increasing dimension of space and with the *degree of nonlinearity of the function studied*. In this context the macroscopic model provides simplifications (incomparable to the complexity of the self-consistent Hartree-Fock or relativistic mean-field approaches) that are inherent to the physical nature of the macroscopic energy problem.

(i) The minimized function, the nuclear macroscopic energy, can be considered a very regular function of its arguments $\alpha_{\lambda\mu}$ in the physical range of their application.
(ii) With the exception of α_{20}, which parametrizes the nuclear elongation, the majority of the deformation parameters remain not very far from the origin $\{\alpha_{\lambda\mu} = 0\}$ of the deformation-space reference frame. They seldom approach 1, except for α_{30} and α_{40}, and even this only at the very large elongations.
(iii) Within the physical range of (so to speak not too "extravagant") shapes, on the average, the larger the multipolarity, the smaller the variation range of $\alpha_{\lambda\mu}$, especially within the near energy range, say, several MeV, from the absolute minimum.
(iv) With increasing multipolarity λ the nuclear surface area increases rather quickly, followed by a rapid increase in the (positive) surface energy. Those latter energy regimes are avoided by the minimization algorithms.

These properties considerably facilitate the use of the minimization algorithm in terms of both the stability of the minimization process converging towards the absolute minimum and the computer CPU time.

In the present approach we employ what is sometimes referred to as *stochastic technique of projections* as briefly described in the rest of this section. It consists of calculating the projections of the total energies on the preselected 2D subspaces, by repeating the minimization starting from randomly selected initial points for every projection point. Possible disadvantages of the stochastic technique of projections have been discussed in Ref. [48] focusing on the case of self-consistent iterative approaches such as the Hartree-Fock method.

In this article we illustrate the LSD calculation results introducing either 1D energy projections and minimizing the energy over various multipole deformations as a function of the elongation α_{20}, or, alternatively, two types of 2D projections. In this second case—to address the issue of the Jacobi shape transitions—we project the total energy on the plane of the leading (quadrupole) deformation parameters $\{\alpha_{20},\alpha_{22}\}$ using, equivalently, the $\{\beta,\gamma\}$ representation. Alternatively, we employ the $\{\alpha_{20},\alpha_{30}\}$ projections minimized over a number of multipole deformations to illustrate the Poincaré-type transitions.

In all the three cases described above we use the Levenberg-Marquardt nonlinear minimization algorithm that is known for its stabilized linear-search properties, which increase an overall stability of the method. In this article, minimization algorithm is combined with the standard multi-restart procedure according to which

(i) the initial minimization points are selected at random in a large hypercube containing, as a rather small subset, the physical space of interest;
(ii) we use $N_{\text{rest.}}$ random restarts to control the obtained consistency and continuity of the final surface (curve) of interest, as well as the independence of the final result of the starting point selected for the minimization routine;
(iii) each time the minimization stops when the zero-gradient condition is verified within the predefined criterion, the consistency of the results obtained from various starting points is analyzed and the solution satisfying the continuity criteria chosen;
(iv) this technique makes it possible, in particular, to detect the mechanism of "crossing valleys" as discussed in Ref. [48]; otherwise, it is very difficult to treat with the help of automatized search routines.

As is well known, stochastic approaches do not offer mathematical guarantees for satisfying the properties for which no mathematical criteria can be formulated. However, using these methods one can increase the probability of reaching a success: *the best one can do under the discussed mathematical conditions*.

In the calculations presented below we employ the minimization over up to 12 deformation coordinates simultaneously with $\lambda_{\max} \leqslant 16$, after having verified that the stability of the final result has been achieved in the context of interest.

Extensive tests of the minimization algorithm applied in the variable dimensions of the deformation spaces used in this article convince us of the absence of possible discontinuities and/or other irregularities in the present context.

IV. EXTENDED LSD-MODEL FORMULATION

In this section we discuss first the properties of the stability of the final results with respect to the spherical-harmonic basis cutoff in terms of the axial symmetry subset of the basis (Sec. IV A) and the axial asymmetry (Sec. IV B). Having examined the convergence properties of the algorithm, we obtain a parametrization of the deformation-dependent congruence-energy term with certain criteria specified below (Sec. IV C), finishing with a few comments about the neck description properties in Sec. IV D.

A. Basis stability conditions: Axial symmetry

Let us recall at this point that the extended LSD energy expression developed in this article contains the deformation-dependent congruence-energy term whose presence strongly influences the quality of the comparison of the nuclear fission barriers with experiment; for illustration, cf. Table VI. When discussing the stability with respect to the basis cutoff in this section we use the full, extended LSD expression, including the deformation-dependent congruence-energy term, despite

the fact that the parametrization of the congruence contribution is presented and illustrated in Sec. IV C only.

We start by examining the conditions of the basis cutoff in relation to the order λ of the spherical-harmonic basis $\{Y_{\lambda\mu}\}$, for the axial-symmetry deformations $\alpha_{\lambda\mu=0}$. Because we are interested, in particular, in the Jacobi shape transitions involving nonaxial (to the first order, triaxial) shapes we specifically illustrate also the role of the higher-order triaxiality degrees of freedom, α_{42} and α_{62}. They can be seen as the "natural partner" deformations possibly coupling with the quadrupole-triaxial deformation α_{22} as discussed in the following section.

An undesirable feature of the description of nuclear surfaces in terms of any set of basis functions is an appearance of *local surface fluctuations*. They, sooner or later, become physically meaningless and yet are an unavoidable consequence of expanding a given function in terms of the basis functions which, one way or another, involve the polynomials of an increasing order. We are confronted here with contradicting tendencies well known in the discussed context. On the one hand, the tendency to increase the basis size to improve the variational minimization conditions and lower the energy of the final solution. This, on the other hand, increases the presence of (to an extent meaningless) small-amplitude fluctuations on the nuclear surface. To examine the behavior of the LSD energy expression as a function of the increasing basis cutoff parameter, $\lambda_{\max}$, we have performed two types of tests.

First, we have tested the total energy behavior as a function of the increasing quadrupole deformation α_{20}, also referred to as the nuclear elongation parameter, at spin zero by minimizing the total energy over the axial-symmetry deformation parameters $\alpha_{\lambda\mu=0}$, for the increasing even-order index λ.

Results in Fig. 1 show the energy differences,

$$\delta E_{\lambda_{\max.}}(\alpha) \equiv E_{\lambda_{\max.}-2}(\alpha) - E_{\lambda_{\max.}}(\alpha), \qquad (15)$$

for $\lambda_{\max.} = 10, 12, 14, \ldots$, for three nuclei representing the mass ranges on which we focus in this article. Because above we subtract the result with the richer basis size from the result with the poorer basis size, the corresponding difference is necessarily non-negative and we keep this convention for the graphical convenience.

It can be seen from Fig. 1 that, between the vanishing deformation at $\alpha_{20} = 0$ and up to a certain value of the elongation which varies from $\alpha_{20} \approx 1.3$ for ^{173}Lu to $\alpha_{20} \approx 1.7$ for ^{70}Se, the discrepancies in terms of the difference $[E_{\lambda_{\max.}=16}(\alpha) - E_{\lambda_{\max.}=18}(\alpha)]$ are of the order of 1 keV and do not exceed 15 keV at $\alpha_{20} = 2$.

In Fig. 1 we have somewhat arbitrarily placed vertical reference lines to mark the points further on referred to as $\alpha_{20}^{\text{stab.}}$. By definition, at these points the discrepancy caused by the strongest-diverging pair of multipolarities is equal to 20 keV. The latter symbol and the reference lines facilitate the discussion below. Observe that the position of the "stability limit," $\alpha_{20}^{\text{stab.}}$, decreases with increasing nuclear mass, as shown in Fig. 1.

Figure 2 (left-hand side) shows the neck radius for the three nuclei discussed as a function of their elongation. The crossing points between the curves and the vertical lines,

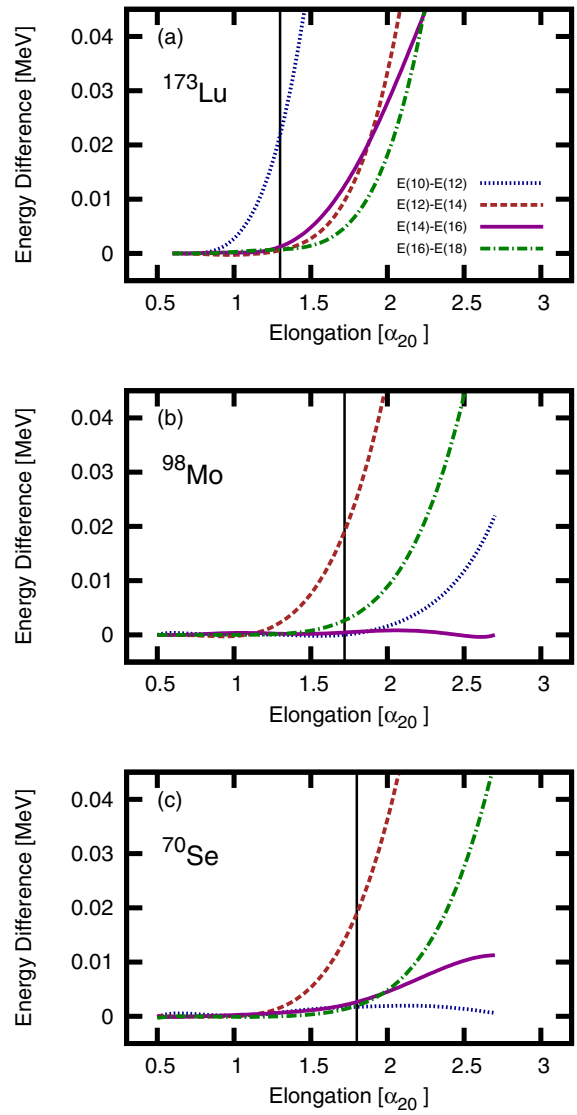

FIG. 1. (Color online) Axial-basis cutoff stability test for three nuclei representative for the mass ranges illustrated in this article. The curves correspond to minimizing the nuclear energy at each α_{20} over other axially symmetric deformations with increasing $\lambda \leqslant \lambda_{\max.}$ Here we select, as a measure of stability, the energy differences in Eq. (15). By definition, vertical lines indicate the elongation at which the biggest contribution equals 20 keV. Observe that, characteristically, the convergence is not monotonic (behavior of the form "the higher the λ value, the smaller the discrepancy" does not apply here). (For comments, see Figs. 2 and 3 and discussion in the text.)

whose positions are copied from Fig. 1, define the "degree" of the neck formation. Recall that for the neck radii in the range, typically (0.3 to 0.4) R_0, the nuclei which are still described with the help of one common surface should rather be considered as effectively two separate nuclear objects, with vanishing probability of returning to the original compact configuration.

Positions of the vertical lines in Figs. 1 and 2 indicate that the basis-instability areas clearly correspond to the advanced stages of the neck formation, and thus further analysis of these instabilities will be focused on the description of the nuclear

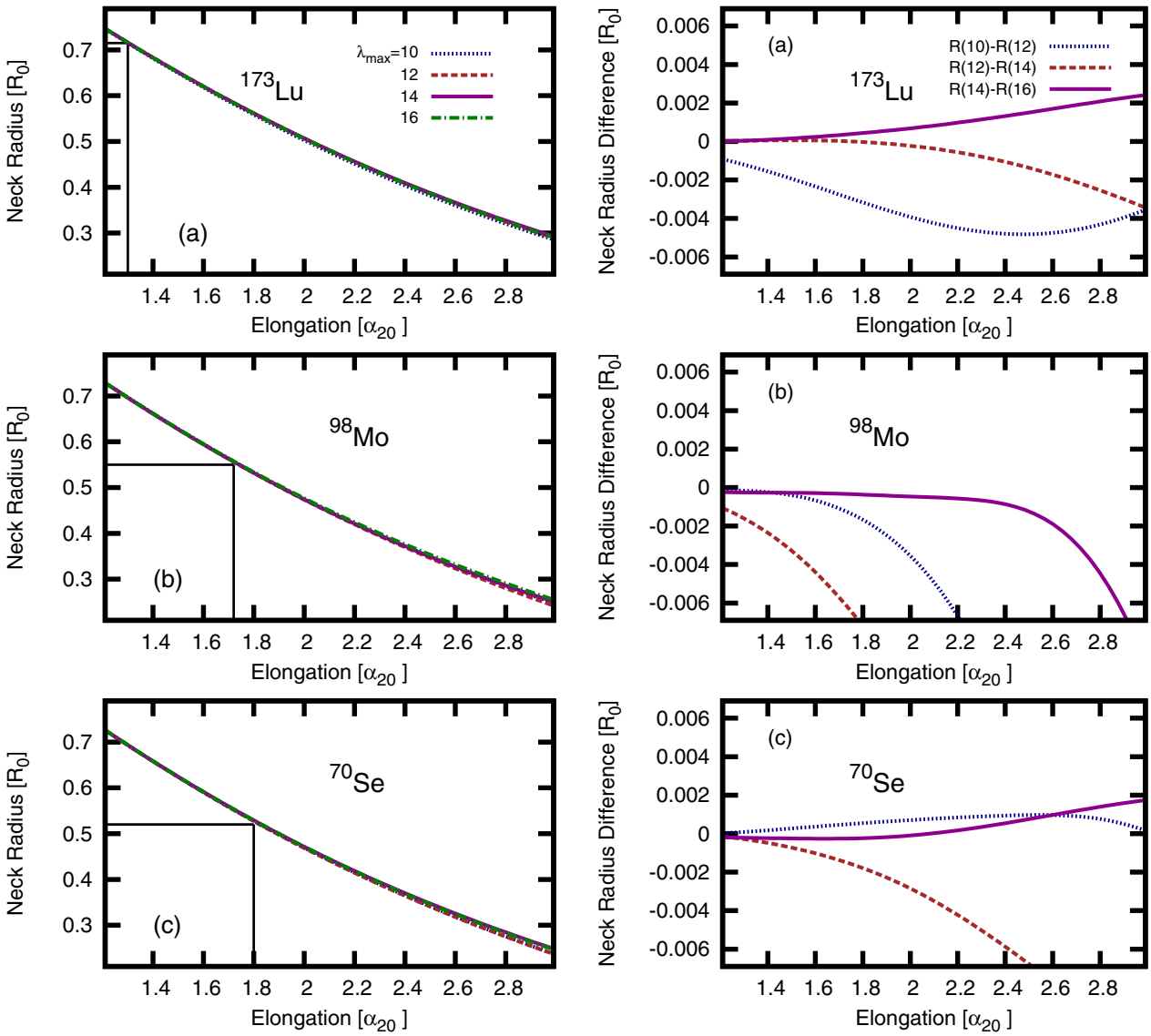

FIG. 2. (Color online) (Left) Neck radius as a function of the nuclear elongation for increasing multipolarity in the nuclear surface expansion, in units of the corresponding spherical radius R_0. Positions of the vertical lines are the same as those in Fig. 1; for more details, see the text. (Observe a perfect stabilization of the nuclear neck-radius curves in terms of the multipole expansion.) (Right) Illustration of the decomposition of the nuclear neck radii in terms of the increasing multipolarity. Observe a nonmonotonic behavior of various contributions with increasing $\lambda_{\text{max.}}$.

neck. This is illustrated in the right-hand side of Fig. 2 by showing the neck-radius contributions coming from various multipolarities. Here, following the convention in Fig. 1, we take as a measure of those contributions the differences between the neck radii obtained with a given $\lambda_{\text{max.}}$ and $\lambda_{\text{max.}} - 2$, denoted symbolically $R(10) - R(12)$, $R(12) - R(14)$, etc. Despite the fact that the neck-radii themselves are pretty robust in terms of the stability of the multipole basis expansion, the detailed contributions of various multipolarities to the neck radius are again not monotonic.

Let us emphasize at this point that from the microscopic point of view, the neck zones are, in fact, the scenes of complex quantum few-body processes in the dilute (decreasing density of) nuclear matter, governed by the two-body and, possibly, three-body correlations, occasionally influenced by the cluster formation, etc. This suggests the existence of a competition among several quantum mechanisms, whose description with the help of classical concepts and a single 2D surface is clearly impossible. Incidentally, the "erratic" fluctuations in question, which could be interpreted as a certain weakness of the spherical-harmonic expansion around the neck zones, as pointed out already in Sec. III C, appear within the area of the limited applicability of the macroscopic energy formula. This limits to an extent the importance of the possible inaccuracies of the multipole expansions in the "neck regime."

It will be instructive to pursue a short discussion of the neck geometry properties within the macroscopic algorithm. The mechanism is further illustrated in Fig. 3 in which the distance x from the nuclear axis $\mathcal{O}_z$ is shown as a function of z for a large value of the elongation. As can be seen from

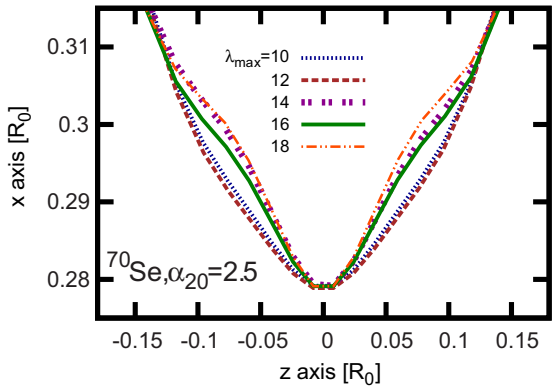

FIG. 3. (Color online) Illustration of the shape fluctuations in the neck region in terms of the increasing order of the axially symmetric multipole contributions for ^{70}Se as an example at $\alpha_{20} = 2.5$. Given the fact that the model cannot claim the adequacy of the description of the neck area at the zone illustrated, the fluctuations shown which remain at the level of 1% of the original radius can be considered "harmless" in the context.

the figure, fluctuations occur with no "evident convergence scheme" behind the order of the curves. Similar neck profiles can be drawn for the smaller elongation, with the conclusion that although the amplitude of the fluctuations decreases with the decreasing elongation, the sequence of the curves on the diagrams of this type does not follow any simple regularity.

From the above illustration and from the results of similar calculations for nuclei in the mass range considered, we conclude that in the deformation regions of the neck formation, the energy contributions of the multipole deformations in excess of $\lambda = 12$ are not monotonic when $\lambda_{\max.}$ increases, but remain small. There exists no reliable way of fitting the model predictions at this point to any observable directly related to the properties of the nuclear neck. Because the macroscopic model cannot assure the adequacy of the description of the dynamics of the neck formation, we believe that the energy fluctuations of this order certainly do not exceed the generic uncertainties of the model itself.

B. Basis stability conditions: Nonaxial shapes

In preparation for the calculations of the Jacobi shape transitions, we have also performed the test calculations at and near the critical spins, using at first the usual $[\{\beta,\gamma\} \leftrightarrow \{\alpha_{20},\alpha_{22}\}]$-plane minimization, but next allowing for the extra minimization over the similar triplanar geometry deformations, α_{42} and α_{62}, at each $\{\alpha_{20},\alpha_{22}\}$ point.

The results corresponding to the "usual" in the present context $\{\beta,\gamma\}$-plane minimization over all the even-λ axial-symmetry deformations $\alpha_{\lambda\mu=0}$ for $\lambda \leqslant \lambda_{\max.} = 16$, however, with neither α_{42} nor α_{62} extra minimization, are given in Fig. 4 for two representative nuclei in the mass range studied. These energy maps are meant to define the energy scale within which the basis cutoff instability tests will be analyzed. The potential energies of Fig. 4 will be labeled E_{22} for further reference, despite the fact that minimization over several axially symmetric deformations is performed at each $\{\beta,\gamma\}$ point.

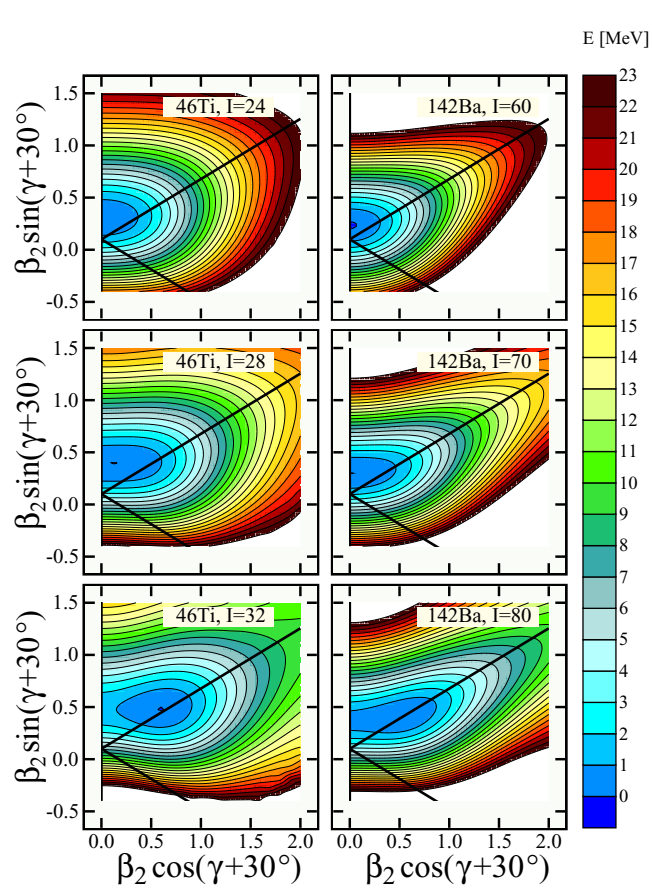

FIG. 4. (Color online) Total energy projections for the nuclei indicated at spins in the vicinity of the Jacobi shape transitions. We use the "traditional" quadrupole deformation parameters (β,γ). The vertical axis corresponds to $\gamma = 60^\circ$ (oblate), with the nuclear spin directed along the symmetry axis. The path to fission ($\gamma = 0^\circ$ axis) has 30° inclination with respect to $\mathcal{O}_x$ axis. Downsloping lines correspond to $\gamma = -60^\circ$, oblate shapes with the nucleus turning about an axis perpendicular to the symmetry axis. Finally, the $\gamma = -120^\circ$ axis corresponds to the prolate shapes with the nuclear spin aligned with the symmetry axis. At each $\{\beta,\gamma\}$ point the energy was minimized over the even-λ deformations $\alpha_{\lambda 0}$ for $\lambda \leqslant 16$.

Next we define two extra energy $\{\beta,\gamma\}$-plane projections. The first one differs from the one illustrated in Fig. 4 in that in addition to the minimization over all even-λ deformations $\alpha_{\lambda\mu=0}$ with $\lambda \leqslant 16$, the minimization over α_{42} is performed at each $\{\beta,\gamma\}$ point. The corresponding energies are denoted by $E_{22,42}$ for short. In the second projection, an extra simultaneous minimization over α_{42} and α_{62} is performed at each $\{\beta,\gamma\}$ point, with the resulting energies abbreviated to $E_{22,42,62}$.

To estimate the impact of the triaxial deformations α_{42} and α_{62}, we constructed the differences of the form $E_{22} - E_{22,42}$ and $E_{22,42} - E_{22,42,62}$, representing the contributions of each single triaxial deformation parameter mentioned. The results of the two energy differences for the lightest among the nuclei considered, ^{46}Ti, are illustrated in Fig. 5, showing no impact whatsoever in the deformation areas surrounding the energy minima. The differences of the order of 200 keV at most represent the energy-gain when minimizing in addition over

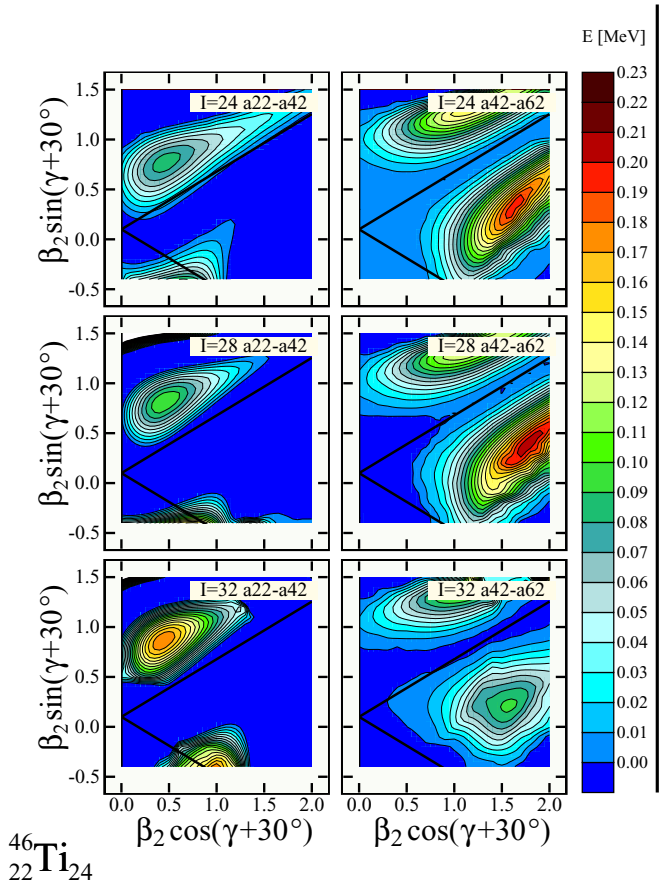

FIG. 5. (Color online) Energy differences for ^{46}Ti at spins, representing the energies from the preceding figure minus the projections minimized in addition with respect to α_{42}, according to the notation introduced in the text: $E_{22} - E_{22,42}$ (left column). The three maps on the right-hand side represent the difference $E_{22,42} - E_{22,42,62}$. Other minimization conditions are same here as in Fig. 4.

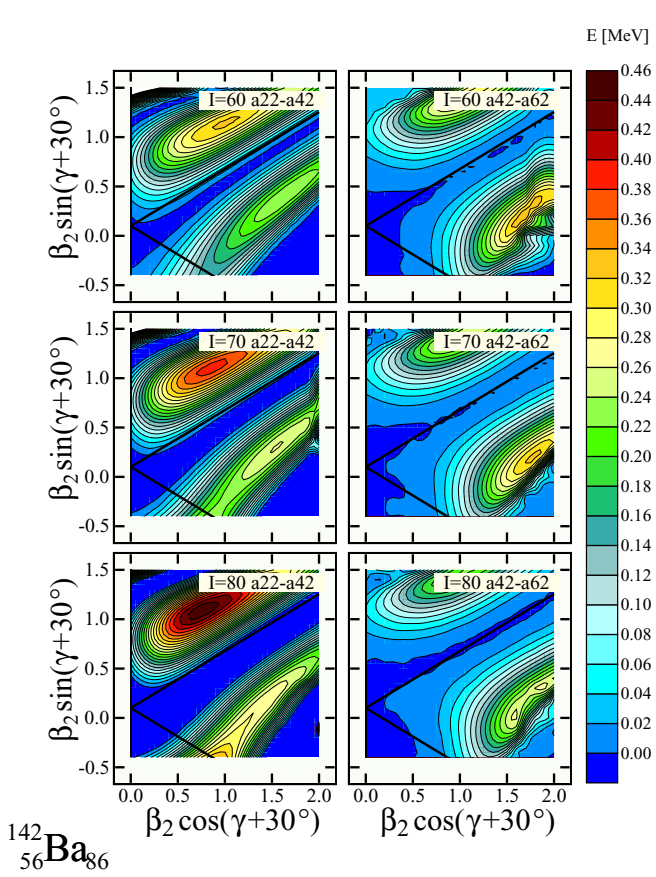

FIG. 6. (Color online) Analogous to the preceding figure, here for ^{142}Ba, representative for heavier nuclei studied in this paper.

the α_{42} deformation. They superpose with the energies at the range of 5 to 10 MeV above the minimum, as can be seen from the left-hand side of Fig. 4. Therefore, they have no impact on one of the central issues in the focus of this article: the dynamical (most probable) deformations that accompany large-amplitude shape fluctuations associated with the Jacobi shape transitions. In the energy scale, the corresponding states are close to the nuclear ground states; i.e., they lie within, approximately, 1 MeV above the potential minimum. A similar conclusion applies for the effect of the α_{62} deformation as seen from the three maps on the right-hand side column in Fig. 5.

For ^{142}Ba representing the heavier-mass nuclei considered in this article, the relative impact of the higher-order triaxial deformations is even weaker. Here the small maxima in Fig. 6 should be compared with the total energies of the order of 15 to 20 MeV above the ground-state minimum. This can be seen directly from the three maps on the left-hand side of Fig. 6 representing the effect of the α_{42} deformation and, similarly from the three maps on the right hand-side of the figure for α_{62}.

Analogous results apply to other nuclei in the mass range considered in this article and we conclude that the effect of the higher-order triaxial deformations α_{42} and α_{62} is negligible for the Jacobi shape transitions in the nuclei studied.

C. Parameterization of the deformation-dependent congruence energy

As mentioned in Sec. II, there exist in the literature a few types of phenomenological assumptions about the form of the deformation-dependent congruence-energy term and, to an extent, they give similar results as far as improvements of the description of the fission barriers are concerned (cf. Refs. [35], [55], or [27]; in the latter the deformation-dependent congruence-energy term of Ref. [35] was used in conjunction with the LSD approach). One of the tendencies in the past was to focus on the parametrizations with possibly a small number of adjustable parameters. To our knowledge, there are no rigorous arguments behind the phenomenological expressions used in the literature. This does not make it possible to construct the clear-cut physics criteria discriminating one approach against the other. Under these circumstances we propose a functional form, in which the only leading idea is to have a certain parametric flexibility making it possible to test the reaction of the model with respect to *"accelerated or slowed-down turning on the congruence term with increasing elongation,"* while improving the description of the fission barrier heights—otherwise, the functional form used below

TABLE VI. Comparison of the barrier heights for the nuclei listed. Columns 2–4 contain Experimental values (Exp.), the reference of the origin (Ref.), LSD model results with the congruence ignored, and the congruence contribution from Myers and Świątecki (denoted C. M.-S.) [35]. The last three columns represent the results obtained using the hypotheses $a_{\rm neck} = 0.5,\ 1.0$, and 1.5.

				α_{20}^0 A-dependent		
Nucleus	Exp. Ref.	No. C.	C. M.-S.	$a_{\rm neck} = 0.5$	$a_{\rm neck} = 1.0$	$a_{\rm neck} = 1.5$
^{70}Se	39.4 [59]	50.618	43.337	38.973	40.393	41.825
^{76}Se	44.5 [59]	54.323	49.624	43.944	45.084	46.068
^{75}Br	41.0 [60]	52.603	47.062	42.169	43.410	44.599
^{90}Mo	42.0 [61]	50.890	45.519	40.995	42.308	43.359
^{98}Mo	46.0 [61]	54.571	50.651	46.495	47.443	48.132
^{173}Lu	29.0 [62]	28.707	25.635	27.433	26.797	26.616
^{228}Ra	6.3 [62]	6.204	6.013	6.204	6.186	6.120

remains an *ad hoc* postulate—similarly to the other forms discussed in the literature.

Below we use the experimental information about the fission-barrier heights in nuclei, in which this information is available, to optimize parameters of the following simple analytical expression here referred to as *neck factor*:

$$F_{\rm neck}(\alpha_{20}) = 1 + \tfrac{1}{2}\left\{1 + \tanh\left[\left(\alpha_{20} - \alpha_{20}^0\right)/a_{\rm neck}\right]\right\}. \quad (16)$$

Above, α_{20}^0 and $a_{\rm neck}$ are two, at this time yet-unknown, adjustable constants. With the above assumption the deformation-dependent congruence-energy contribution are defined as

$$E_{\rm cong.}(N,Z;\alpha) \stackrel{df}{=} W_0(Z,N) F_{\rm neck}(\alpha_{20}), \quad (17)$$

where the so-called Wigner energy term (cf. Refs. [56,57]), denoted W_0, is still parametrized as in Ref. [58], i.e.,

$$W_0(Z,N) = -C_0 \exp(-W|I|/C_0), \quad (18)$$

with $I \equiv (N-Z)/A$, $C_0 = 10$ MeV, and $W = 42$ MeV. The rest of this section is devoted to the description of the determination of the phenomenological parameters, α_{20}^0 and $a_{\rm neck}$, of the nuclear neck formation.

For the present applications it is convenient to introduce an A dependence through a simple linear form, i.e., $\alpha_{20}^0 \to \alpha_{20}^0(A)$, in which we "arbitrarily parametrize the α_{20}^0 parameter" as a function of the mass number

$$\alpha_{20}^0(A) = \alpha_{20}^{\rm min.} + \frac{\left(\alpha_{20}^{\rm max.} - \alpha_{20}^{\rm min.}\right)}{\left(A^{\rm max.} - A^{\rm min.}\right)}\left(A - A^{\rm min.}\right), \quad (19)$$

where $\alpha_{20}^{\rm min.}$, $\alpha_{20}^{\rm max.}$, $A^{\rm min.}$, and $A^{\rm max.}$ are predefined *a priori* as

$$\alpha_{20}^{\rm min.} = 1.5, \quad A^{\rm min.} = 70, \quad (20)$$

$$\alpha_{20}^{\rm max.} = 3.5, \quad A^{\rm max.} = 220, \quad (21)$$

so that effectively only the $a_{\rm neck}$ parameter can be seen as a truly adjustable constant.

By repeated minimization of the nuclear macroscopic energy over the multipole deformation parameters $\alpha_{\lambda 0}$ with $\lambda \in [3,16]$ as a function of the elongation, α_{20}, for various parameter values of $a_{\rm neck}$, we have verified that the values $a_{\rm neck} = 0.5, 1.0, 1.5$ presented in Table VI can be considered as an acceptable approximation when minimizing the discrepancies between the model and the experimental fission barriers.[5]

The LSD model energy expression in Eq. (1), together with the modification which aims at including the deformation-dependent congruence-energy term, Eqs. (16) and (17)–(21), is referred to as LSD-C, with "C" standing for "congruence."

D. Some more comments about the nuclear neck

The very notion of the nuclear neck is, of course, a fully classical, geometrical concept in the present approach. As is well known, the nuclear mean-field interaction can be parametrized phenomenologically using, e.g., the Woods-Saxon potentials with the diffusivity parameter $a \approx 0.6$ fm. With the latter value, the nuclear skin thickness defined as the distance for which the potential decreases from 10% to 90% of its minimal value, corresponds to $4\,a \approx 2.5$ fm. In other words, the radius value at which the potential falls to its 90% of the minimum value is $R_{90\%} = R - 2a \approx R - 1.2$ fm.

Let us consider a nucleus with $A = 125$ nucleons for which the radius estimated as usual is $R = r_0 A^{1/3}$, which with $r_0 = 1.2$ fm gives $R = 6$ fm. At the neck value of the order of $0.4 \times R = 2.4$ fm, the Woods-Saxon potential is equal to its 90% depth at $R_{90\%}^{0.4} \approx (2.4 - 1.2)$ fm, ≈ 1.2 fm, which is of the order of *the half of the nucleon size*. We conclude that there is no way that the macroscopic model with the concept of the classical surfaces can approach any realistic description of this part (neck) of the nucleus.

When the neck radius approaches this range, one may say that the spatial nucleonic content of this part of the nucleus is "merely composed of the nuclear skin" and that the corresponding configuration nears the scission configuration. As already mentioned, for heavy and moderately heavy nuclei the corresponding typical neck size for deformations neighboring the scission configuration can be expressed, rather roughly, as $R_{\rm scission} \approx (0.3 - 0.4)\,R_0$, where $R_0 = r_0\,A^{1/3}$ and where $r_0 \approx 1.2$ fm.

[5]The experimental values in Table VI have been obtained similarly as in Ref. [35], i.e., subtracting the shell-energy contribution at spherical shapes and using the fact that the shell energies at the saddle points can be considered negligible according to Świątecki's "topological property."

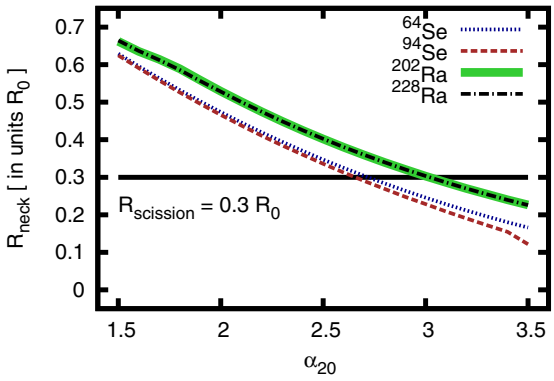

FIG. 7. (Color online) Neck radii of the nuclei indicated as a function of the quadrupole deformation. Plotted values are normalized to the radii of the corresponding spherical nuclei, the former defined by $R_0 = r_0 A^{1/3}$, with $r_0 = 1.2$ fm. The horizontal line shows the geometrical scission reference defined by $R_{\text{scission}} = 0.3R_0$. Let us emphasize that the latter quantity can be seen as a somewhat arbitrary reference value.

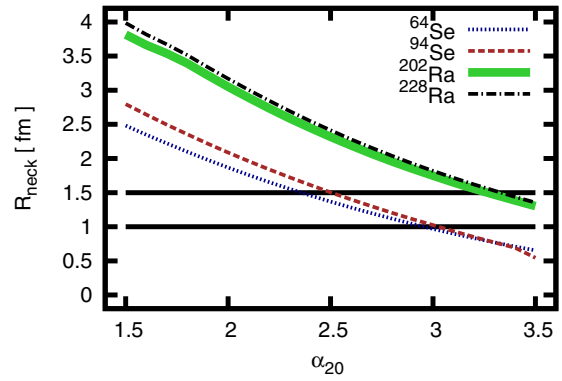

FIG. 8. (Color online) Illustration similar to the one in Fig. 7, but with the neck radius expressed in fm. At the level of the neck size of the order of 1.5 fm, there is hardly any space left for any single nucleon to move orthogonally with respect to the elongation axis.

In what follows it is instructive to obtain a global information about the neck evolution with increasing quadrupole deformation α_{20}, which, within the multipole parametrization of the nuclear surface used in this article, is a leading component in describing the nuclear elongation. To obtain such an illustration, we have calculated, as before, the total nuclear energies for increasing α_{20} for a few nuclei for which the experimental data on the fission barriers exist in the literature. Figure 7 shows the neck radii relative to the radius of the equivalent spherical nucleus, as a function of the nuclear elongation obtained by using the same calculations as the ones used to obtain Fig. 1. In this case, $R_{\text{neck}} = x$ at $z = 0$.

Curves obtained without taking into account the deformation-dependent congruence energy coincide with the ones with the deformation-dependent congruence-energy included and therefore in the figure we place only one set of them. Let us emphasize here that the process of the creation of the nuclear neck on the way to fission (referred to as "necking") depends very little on the mass number, A, and even less on the nucleon excess $|N - Z|$, as results in Figs. 7 and 8 indicate.

The neck radii of the corresponding selected nuclei, illustrated in the figures, decrease almost linearly with the quadruple deformation, the negative slope depending only slightly on the mass of the nucleus at least in the cases examined. To verify that these results, do not depend very much on the isospin we have included in the comparison with the nuclei with relatively large differences in the nucleon excess, $N - Z$.

As can be seen from Fig. 7, in the light nuclei such as ^{64,94}Se, the neck radius approaches R_{scission} for the elongation of $\alpha_{20} \approx 2.5$ at the most, probably markedly earlier. For heavy nuclei, represented by radium isotopes, the neck radius approaches the discussed limit at higher quadrupole deformation of $\alpha_{20} \approx 3$ or slightly earlier.

In the selenium case, the isospin dependence is practically nonexistent; as seen from Fig. 7, one cannot distinguish among the positions of the illustrated curves for the span in the neutron number of $\Delta N = 30$. Let us notice that the results concerning the neck description, but obtained using the Myers-Świątecki prescription, are indistinguishable from the ones presented within the scale of the plot.

V. DEFORMATION DEPENDENCE OF THE FISSION BARRIERS

We use the experimental fission barrier heights to compare with the model results of the optimized, here LSD-C, approach for ^{70,76}Se [59], ^{90,98}Mo [61], and ^{173}Lu [62]. Our results are compared with those of Ref. [58], showing an alternative parametrization of the deformation-dependent congruence-energy term.[6]

Let us begin by illustrating the obtained parametric dependence of the LSD-C realization of the model in terms of the parameter a_{neck}, the latter controlling the way (smoother vs more abrupt) the congruence-energy contribution lowers the barrier when elongation increases. The corresponding results are given in Fig. 9, where the fission barriers at $L = 0$ (no rotation) are shown. These results were obtained at each given elongation α_{20} by minimizing the nuclear energy over 10 deformation parameters[7] $\alpha_{\lambda 0}$, with $\lambda \in [3,12]$. In what follows we compare the results obtained for three values of the "neck-parameter," $a_{\text{neck}} = 0.5$, 1.0, and 1.5.

Adopted parametrization of the congruence-energy contribution lowers the nuclear fission barriers in a way that is rather independent of the neutron excess down to the scission point. The improvement brought by the congruence term is $\delta E \approx -10$ MeV for the light nuclei studied. Let us notice that

[6]Let us remark in passing that the experimental macroscopic barriers for the lightest nuclei cited here are deduced from the corresponding excitation functions and are dependent on the level density parameter used in this type of analysis. Uncertainties in the level density parameters may influence deduced fission barrier heights by a few MeV.

[7]Although the odd-λ multipoles have been formally allowed in the minimization, the final results depend only on the even-λ deformations.

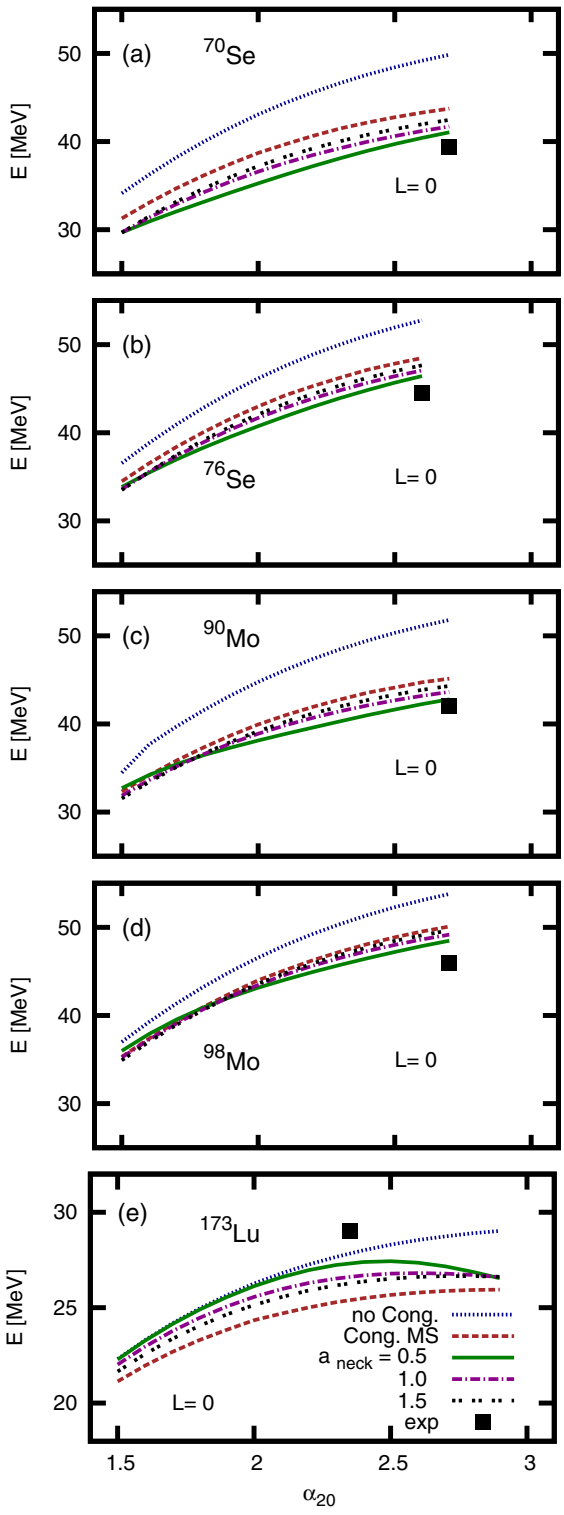

FIG. 9. (Color online) LSD-C model energies as functions of α_{20}, minimized over $\{\alpha_{\lambda 0}\}$ for $\lambda \in [3,12]$ for the $a_{\rm neck}$ values indicated, compared with the energies from of Myers and Świątecki [58] and labeled (Cong. MS). Experimental values, squares, from the references given in Table VI are placed at either the scission elongations defined by the condition $R_{\rm neck} = 0.3 \times R_0$ (all but one), or the saddle-point deformation in the case of ^{173}Lu; cf. the text for more details).

our results with $a_{\rm neck} = 0.5$ are the closest to the experiment, with the typical discrepancy of the order of 1 MeV, the model overestimating the experimental values for all the nuclei except for ^{173}Lu. In the latter case the LSD-C result underestimates the experimental value, but is close to it.

The LSD-C energy curves extend *formally* to the very high elongation values in terms of α_{20}. However, the scission point defined conventionally by the condition that $R_{\rm neck} \approx 0.3\, R_0$, quite often sets in for markedly smaller α_{20} values; cf. discussion in Sec. IV D. The corresponding effect is illustrated in Fig. 9, in which the experimental values of the fission barriers (solid squares) are placed, by convention, at the scission-point elongation. We consider the nuclei at this stage of their shape evolution as *effectively* composed already of two fragments.

At this stage, a realistic description of the processes taking place in the neighborhood of the scission configuration may sensitively depend on the orbitals available at the Fermi level(s) (of the mother and daughter nuclei) and one may expect that the fully quantum description is needed. Under these circumstances a nuclear quantum many-body theory, e.g., self-consistent Hartree-Fock or self-consistent relativistic mean field approach is expected to generate the relevant microscopic ingredients such as the single-particle wave-functions. The latter are needed to describe the possible cluster formation or other mechanisms in the neck zone, which in turn would strongly depend on the nucleus.

We do not believe that our macroscopic-model energy formula has the necessary ingredients to provide a correct description of the total nuclear energy under the discussed circumstances. Therefore, the illustration in Fig. 9 represents most of the curves (all but the one for ^{173}Lu) in such a way that they terminate, by definition, at the conventionally defined scission points. Interestingly, the results of Ref. [58] overestimate (underestimate) the experiment in the same nuclei in which the LSD-C overestimates (underestimates) the data. In absolute terms, the LSD-C provides an improvement by at least a factor of 2 (4 on average), as compared to the above-cited reference.

VI. BASIS CUTOFF, NUCLEAR POTENTIAL ENERGIES, AND ENERGY MINIMA

We illustrate the reaction of the LSD-C energy formula induced by adding more and more terms in the spherical-harmonic basis. Let us observe in passing, that in certain applications, enlarging the basis may be considered of a strong disadvantage and/or even a prohibitive step as in the description of the motion in terms of, e.g., Langevin equations. Indeed, in this case the increasing number of differential equations which need to be solved could represent a prohibitive aspect of such methods. Although in such situations alternative parametrizations of nuclear shapes may be preferable, yet in any case, testing those alternative parametrizations must pass by the basis cutoff ultimate verification to guarantee that such an alternative is indeed acceptable.

Because the evolution of the nuclear shapes with spin is one of the main interests here, we included the angular momentum dependence in the tests.

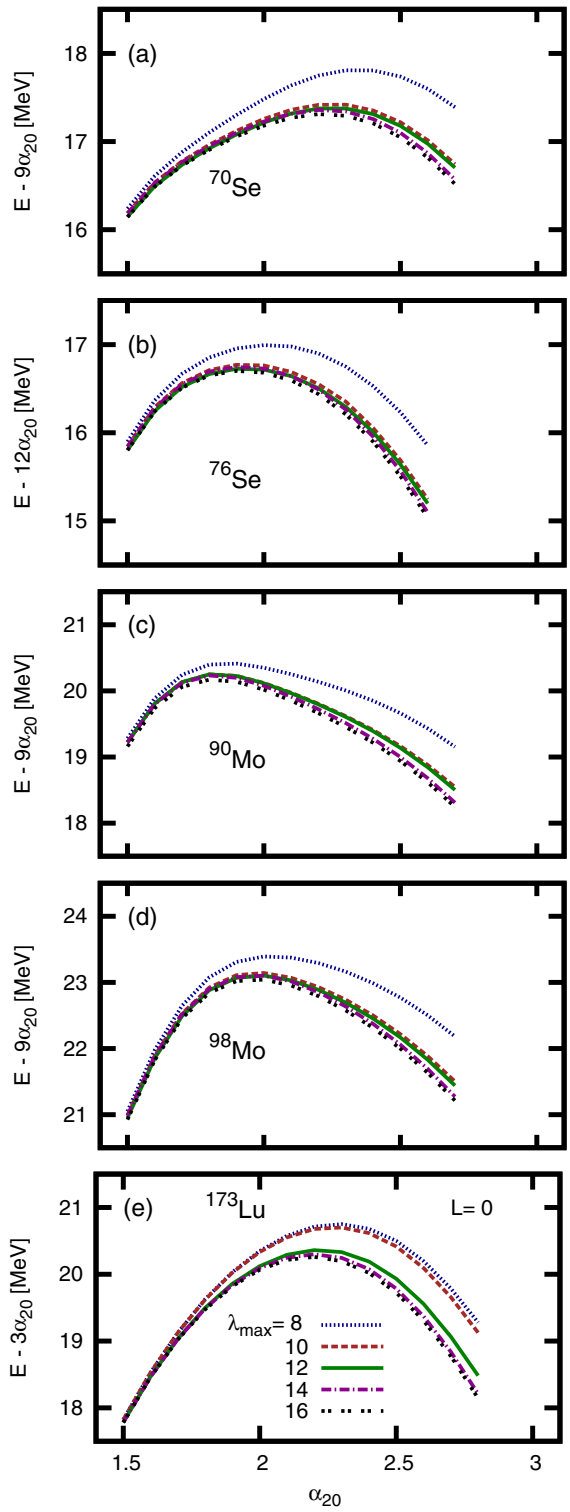

FIG. 10. (Color online) Dependence of the nuclear energy calculated using the LSD-C expression with $a_{\text{neck}} = 0.5$ at the large elongation regime and at spin $L = 0\ \hbar$, as a function of the basis cutoff. The energies have been minimized over deformations $\alpha_{\lambda 0}$ for $\lambda \leqslant \lambda_{\text{max}}$ indicated. To increase the legibility of the present illustration, a linear reference has been subtracted as indicated in the description of the vertical axis. By convention, the curves stop at the deformation at which $R_{\text{neck}} < 0.3 \times R_0$ for all but the ^{173}Lu case, in which the saddle-point deformation comes first.

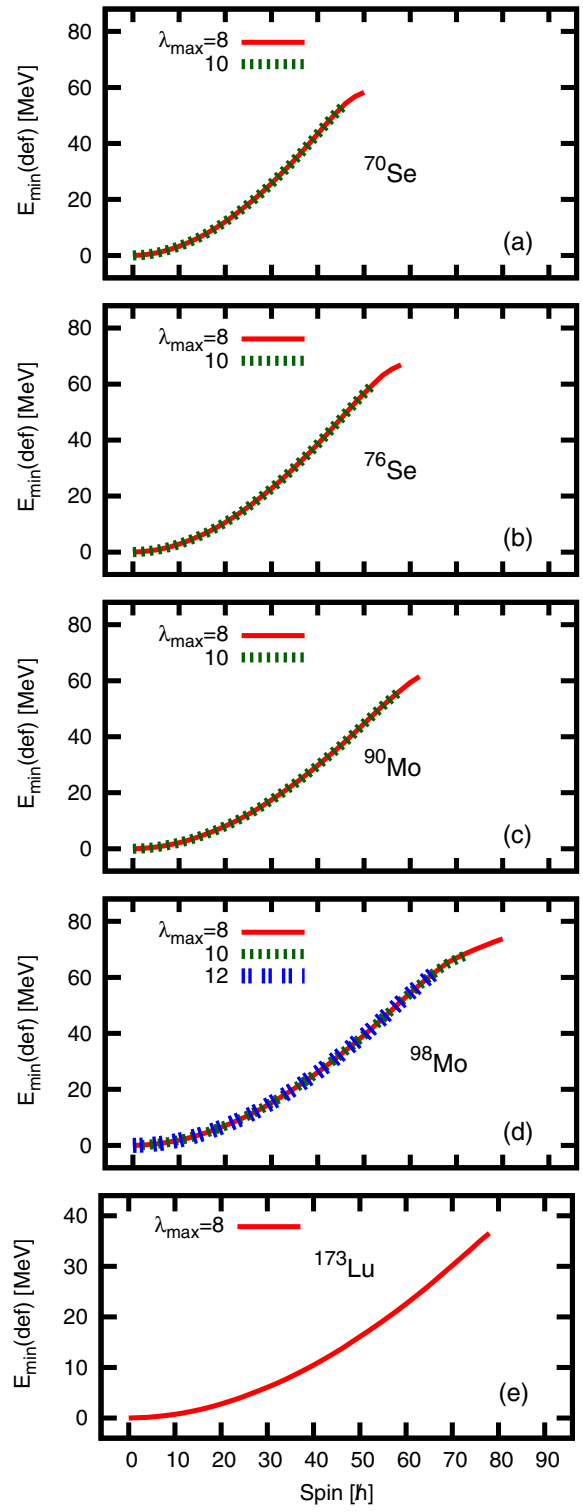

FIG. 11. (Color online) Dependence of the nuclear minimum energy on the basis cutoff parameter λ_{max} as indicated as a function of increasing spin. Minimization performed over $\alpha_{\lambda 0}$ for $\lambda \leqslant \lambda_{\text{max}}$. The macroscopic energies include the shape-dependent congruence energy with $a_{\text{neck}} = 0.5$. Curves end if the scission condition is met for spins lower than the spins at which the barrier vanishes, otherwise at the spins of the vanishing barriers. Notice that the stability is obtained already at $\lambda_{\text{max}} = 8$.

Figure 10, in which the static ($L = 0\hbar$) nuclear energies are plotted for various cutoff parameters $\lambda_{\max}$, illustrates the impact of the basis cutoff on the total nuclear energy along the path to fission. As can be seen from the figure the strongest impact is expected at the largest elongation, with $\alpha_{20} \approx 2.5$: There, increasing $\lambda_{\max}$ from 12 to 14 may lower the energy by not more than about 100 keV. It should be emphasized at this point that for better legibility of the figure, the total energies are plotted after having subtracted a smooth linear reference curve, as indicated and consequently the maxima in those curves *do not* represent the positions of the saddle points (fission barrier heights).

Results of the analogous tests are shown in Fig. 11 for the absolute *minima* of the potential energies. There the main effect of the basis cutoff manifests itself in lowering the critical (scission or saddle) spin values with increasing $\lambda_{\max}$ (recall that the saddle-point elongation α_{20} is in all but the ^{173}Lu case larger than the elongation corresponding to the scission condition introduced and discussed above). The stability of the final results for the numerical values of the *energy minima* is achieved already at $\lambda_{\max} = 8$ for all the cases studied.

VII. NUCLEAR YRAST ENERGIES AT INCREASING SPIN

Within classical nuclear models the nuclear rotation is usually accounted for by adding to the spin-independent macroscopic energy the classical rigid-body rotational-energy term, in the form of Eq. (8), with the rigid-body moment of inertia, $\mathcal{J}(N,Z;\alpha)$, calculated using the uniform nuclear density distribution corresponding to nucleons contained within the surface given by Eq. (14). To calculate the lowest rotational energy, one uses the rotation axis associated with the largest moment of inertia, thus providing the lowest energy contribution.

Some authors calculate the moments of inertia using the diffused-surface assumption (cf., e.g., Ref. [31]), which is more physical. However, the relatively small differences that result can be at least partially accounted for by possibly readjusting the nuclear radius constant r_0. To illustrate the order of magnitude of variations/uncertainties possibly caused by the freedom in choosing the radius parameter when reproducing the values of the classical moment of inertia (and to convince ourselves about the possible sizes of these uncertainties) we compare in Fig. 12 the results obtained for three characteristic values of the r_0 parameter. The results show that only at the deformations very close to the fission/scission can some "slightly visible impact" of the radius uncertainty be expected.

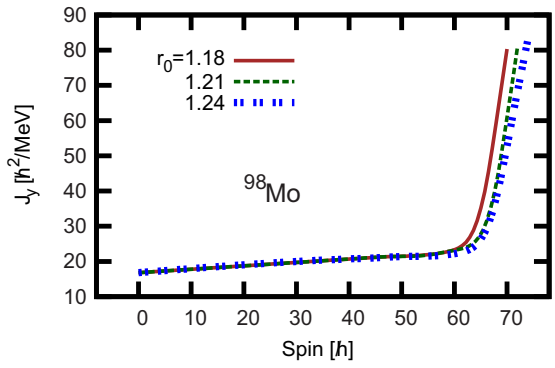

FIG. 12. (Color online) Illustration of the typical behavior of the classical moment of inertia at the deformations corresponding to the minimum of the potential energy for increasing spin, at three typical values of the nuclear radius parameters r_0; for details, see the text and Fig. 11. Results for other nuclei have very similar form.

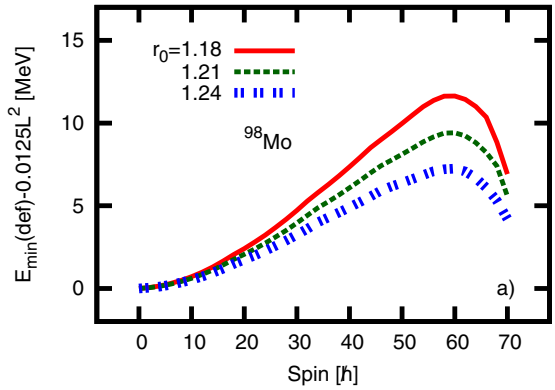

FIG. 13. (Color online) Illustration of the typical impact of the uncertainties in the classical nuclear moments of inertia on the total energy minimization result—here in terms of the total energies at the nuclear energy minima for the three radius-parameter values indicated—plotted relative to a parabolic reference to increase the legibility of the figure.

Because the moment of inertia has a direct impact on the total energy description, and thus the description of the shape transitions, we illustrate in Fig. 13 the results analogous to the ones in Fig. 11. In this article we are using the radius parameter value $r_0 = 1.21$ fm. The variation of r_0 within ± 0.03 fm, which can be considered already very large in the context, leads to about ± 2 MeV absolute shifts in terms of the total minimum energies at the highest spins. However, the latter dependence influences the total energy surfaces in a very smooth, regular, and easily foreseeable manner, its impact being mainly to lower or increase the slope of the yrast lines.

Figure 14 presents the dependence on spin of the scission-point energies or the saddle-point energies, calculated with (dashed lines) and without (solid lines) congruence-energy contribution. Because the congruence-energy contribution is negative and its value decreases (increases in absolute terms) when the nuclear deformation approaches scission, the barrier heights calculated with the congruence-energy contribution are systematically lower.

VIII. LARGE-AMPLITUDE EFFECTS IN NUCLEAR SHAPE TRANSITIONS

In this section we present the problem of the nuclear large-amplitude motion for spins in the vicinity of the transition critical spins. We begin with the Jacobi-type transitions and present the Poincaré shape transitions next. As it turns out, all other shape transitions can be treated in a similar manner.

As already mentioned, our goal is, among others, to investigate the competition between the nuclear Jacobi- and

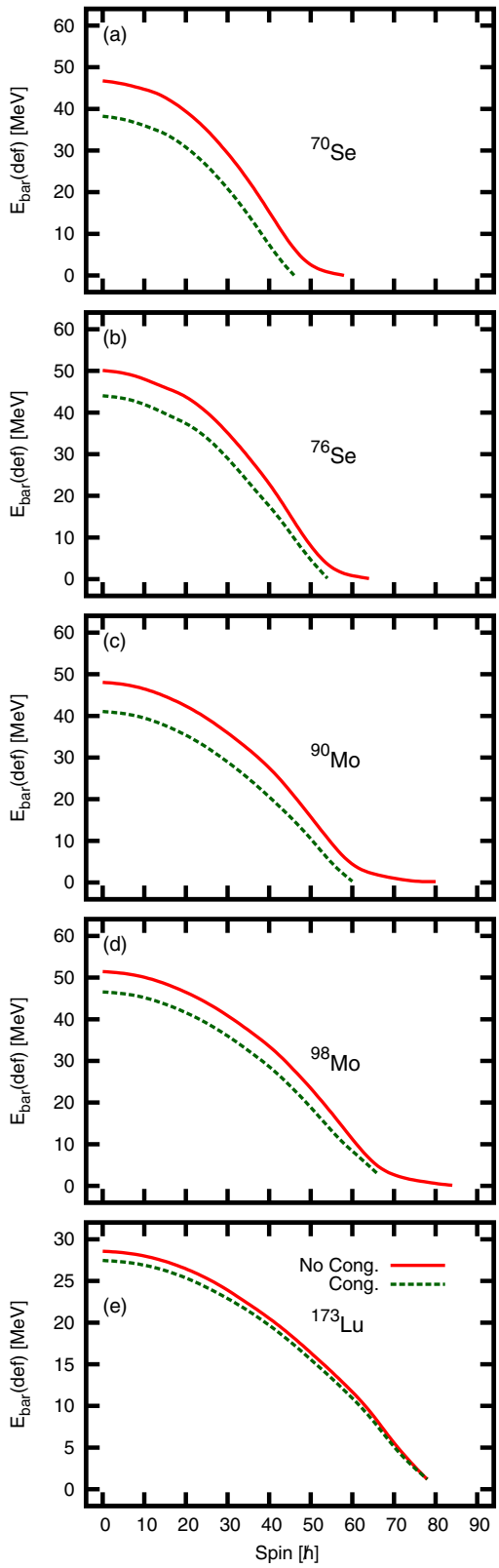

FIG. 14. (Color online) Fission barrier heights obtained with (dashed line) and without (solid line) congruence-energy contributions by using, in the former case, $a_{neck} = 0.5$. The barrier heights are defined either as the nuclear energy at the scission point—if the saddle point corresponds to the stronger elongation (compared to the scission point)—or else to the saddle-point energy.

Poincaré-type shape transitions with increasing spin at high temperature. The experimental signals of the Jacobi shape transitions are relatively indirect, but can be detected, for instance, by investigating the shape of the GDR as a function of the nuclear spin [11–15,17–19]. Poincaré shape transitions, in turn, consist of shape transformations that break the left-right symmetry, thus leading to the asymmetric fission-fragment mass distributions. The experimental tests in question may require very distinct instrumental conditions to address each of the discussed mechanisms separately. Their combination, while performing independent measurements, may be necessary for testing the theoretical model predictions and obtaining more precise information and a more complete understanding of the underlying nuclear properties.

The critical spins of the nuclear shape transitions of interest are defined as follows. In the framework of the static description, the Jacobi critical-spin value, $L_J^{\text{crit.}}$, is given by the first spin at which the absolute energy minimum corresponds to a nonaxial deformation. Similarly, within the static description of the Poincaré shape transitions, the Poincaré critical-spin value, $L_P^{\text{crit.}}$, is defined as the first spin at which the absolute energy minimum corresponds to a left-right asymmetric shape.

Calculations show that the congruence-energy term, in addition to systematically lowering calculated nuclear energies, also lowers the critical spins for both the Jacobi and the Poincaré transition.

A. The case of the Jacobi transitions

When approaching the critical-spin value for a given type of the shape transition, the corresponding energy landscape flattens, often forming characteristic "valleys" in subspaces of two or more dimensions in the multidimensional deformation space. Typical results of the LSD-C calculations for the Jacobi shape transitions with the energy minimized in multidimensional deformation spaces are illustrated using 2D projections in Figs. 15 and 16. The main purpose of comparing these two figures is to provide a translation from the often applied $\{\beta,\gamma\}$ representation of Bohr and an alternative, $\{\alpha_{20},\alpha_{22}\}$ representation, in which the two quadrupole shape coordinates appear at the same footing. In the case of the Bohr parameterization with (β,γ) parameters, the first of the two has the geometrical interpretation of the radial distance from the origin of the reference frame, whereas the other one has that of the polar angle. In the case of the considered alternative, $\{\alpha_{20},\alpha_{22}\}$ are the expansion coefficients in front of the corresponding spherical harmonics. This latter representation will be of advantage when solving the Schrödinger equation for the collective motion, the main subject of this section.

Referring to the results in Figs. 15 and 16, let us observe a gradual displacement of the absolute minimum along the oblate-shape axis ($\gamma = 60^\circ$ vertical axis according to the convention of Fig. 15 and the positive-inclined axis according to the convention of Fig. 16) at $L = 50$–$60\ \hbar$, followed by the transition towards increasing α_{20} with the triaxiality increasing at first (in other words, angle γ decreasing from 60° towards $\gamma \approx 0^\circ$ with the triaxiality reaching its maximum at $\gamma = 30^\circ$) when spin increases. Observe that, according to the calculations, at spins $L = 80$–$84\hbar$, the nucleus arrives at the

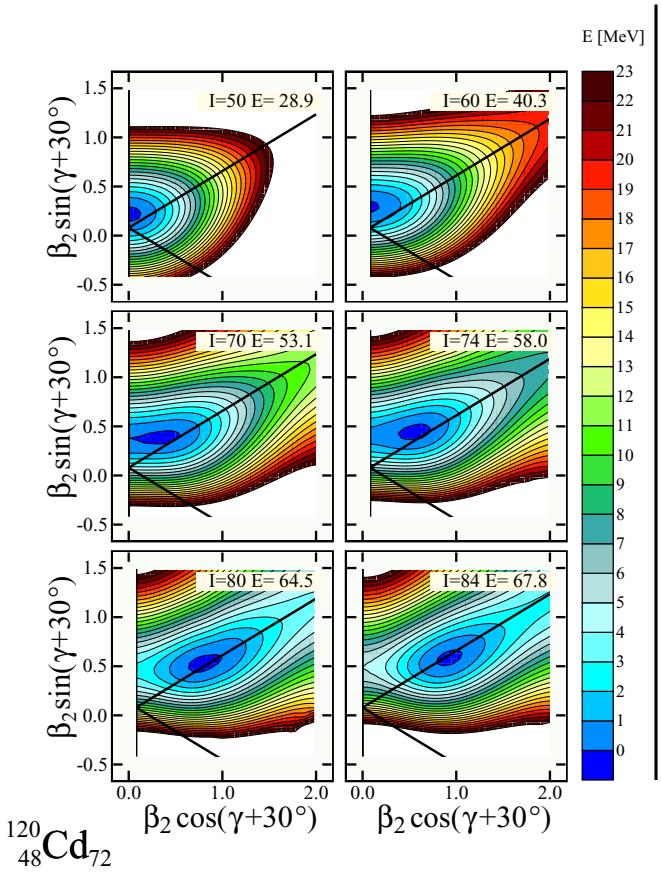

FIG. 15. (Color online) Total energy surfaces for increasing spin in ^{120}Cd, using a "traditional" shape-coordinate representation with the quadrupole deformation parameters (β,γ) of Bohr. The vertical, upsloping straight lines correspond to $\gamma = 60^\circ$ (representing oblate shapes, with the spin of "noncollective" origin aligned with the symmetry axis), whereas the "path to fission" ($\gamma = 0^\circ$ axis) has 30° inclination with respect to the $\mathcal{O}_x$ axis. Downsloping straight lines correspond to $\gamma = -60^\circ$ deformation and represent oblate shape configurations in which the nucleus is rotating collectively about an axis perpendicular to the symmetry axis. Finally, the vertical, downsloping axes correspond to prolate axially symmetric configurations with spins aligned with the symmetry axis. (The minimization over axial-deformation coordinates $\alpha_{\lambda 0}$ with $\lambda \leqslant 12$; the insets contain the actual spin and the energy minimum in MeV using the normalization to zero at $I = 0\hbar$.)

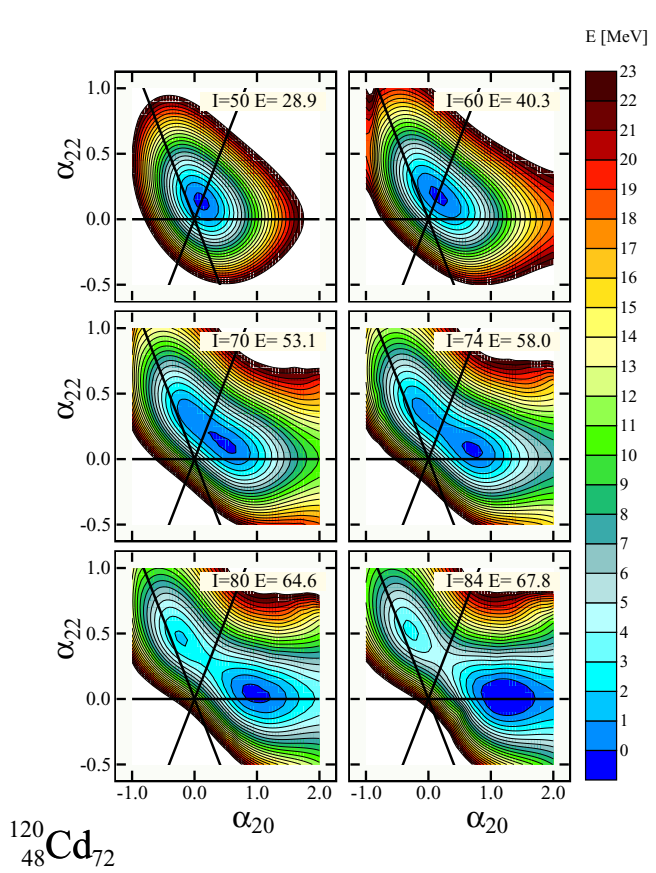

FIG. 16. (Color online) Illustration equivalent to the one in Fig. 15 but using an alternative set of coordinates, α_{20} and α_{22} rather than β and γ, the former better suited for the formulation of the equations of motion of the collective model (discussed here and in the next section). [These coordinates make it possible to write the kinetic energy operator in the Hamiltonian of Eq. (11) in a convenient uniform fashion.] Surfaces of the potential energy, for spins around the critical-spin value for the Jacobi shape transition in ^{120}Cd, minimized over the axial-deformation parameters $\alpha_{\lambda 0}$ with $\lambda \leqslant 12$. Compared to Fig. 15, horizontal lines correspond to $\gamma = 0^\circ$ (axial) deformation, the straight lines with the positive inclination correspond to the $\gamma = 60^\circ$ axis, whereas the line with the negative inclination corresponds to the $\gamma = -60^\circ$ axis. Prolongation of each of the axes on the opposite side of the center corresponds to changing the geometry: oblate $\rightarrow$ prolate and vice versa.

axial quadrupole deformation, $\alpha_{20} \approx 1.0$, with the triaxiality $\alpha_{22} \approx 0$, i.e., a strongly elongated, almost axially symmetric shape with $\gamma \approx 0^\circ$, marking a gradual termination of the Jacobi transition in this nucleus.

Despite the fact that the *model* used here to calculate the nuclear macroscopic energy is classical, the physical system is not, and therefore the motion of the latter in the deformation space should be described using the nuclear collective model, Sec. III A, whose Schrödinger equation can be written in the usual form,

$$[\hat{T} + \hat{V}(\alpha)]\Psi_N(\alpha) = E_N\,\Psi_N(\alpha). \qquad (22)$$

Above, the kinetic energy term, $\hat{T}$, depends on the inertia (mass) tensor; cf. Eq. (11). The latter, at low nuclear temperatures, is, in general, a complicated object depending nontrivially on the deformation coordinates through the single (quasi)-particle energies and wave functions, thus reflecting the quantum shell effects.

The potential, $\hat{V}(\alpha)$, with the single symbol α standing for *all* the deformation coordinates used, represents the same nuclear energy whose 2D projections are illustrated in the figures throughout this article. Let us recall that determining $\hat{V}(\alpha)$ with the help of a macroscopic model alone, as in the case of the present article, can only be a realistic approximation at

TABLE VII. The irrotational flow mass parameter $B_{\text{irr.}}$ as an estimation believed to be better than just the order-of-magnitude estimate. We use Eq. (23), and $R_0 = r_0 A^{1/3}$ with $r_0 = 1.2$ fm.

Nucleus	B_{irr}
^{46}Ti	2.54
^{88}Mo	8.06
^{120}Cd	13.5
^{128}Ba	15.0
^{142}Ba	17.9
^{147}Eu	18.9

relatively high nuclear temperatures, sufficiently high that the quantum shell effects can be considered already washed out.

For the same reasons, as is well known, the shell effects on the inertia tensor can be considered negligible at sufficiently high temperatures;[8] cf., e.g., Fig. 5 in Ref. [63] and references therein. This justifies, as an approximation, setting the corresponding inertia components constant in the present context, which simplifies considerably the numerical effort without having an important impact on the main goal of this article: to illustrate the influence of the flatness of the potential valleys and the large-amplitude motion in the case of the critical shape transitions, as compared to the purely static description.

It has been verified through the calculations (cf. the reference cited above for an illustration) that the so-called irrotational flow expression of the mass-tensor quadrupole component corresponding to the nuclear elongation,

$$B_{\alpha_{20},\alpha_{20}} \approx B_{\text{irr.}} \approx \frac{2}{15} M A R_0^2, \tag{23}$$

provides results that are close to the microscopic ones at temperatures in excess of 1 MeV, which corresponds to the range of interest in this article. Table VII provides the corresponding estimates for a few nuclei in the mass range discussed in this article. To our knowledge, not much is known about the mass-tensor components other than $B_{\alpha_{20},\alpha_{20}}$, the latter calculated using various approximations essentially in the context of the 1D estimates of the fission lifetimes, and even less is known about that at high temperatures. Under these circumstances, to obtain the first approximation of the behavior of the collective wave functions around the total energy minima, the latter evolving as the functions of spin, we have set, as an approximation, $B_{\alpha_{22},\alpha_{22}} = B_{\alpha_{20},\alpha_{20}}$, and neglected the mixed term, $B_{\alpha_{22},\alpha_{20}} = B_{\alpha_{20},\alpha_{22}}$. In our opinion, such an approximation provides a good overall orientation as far as the evolution of the spreading of the nuclear wave functions in function of spin is concerned, especially as the first (nonstatic) calculations of this kind for the nuclear shape transitions of the Jacobi type.

[8]The nuclear temperatures at which the quantum shell effects are "washed out" depend to an extent on the nuclear mass range and the possible closeness of the actual Fermi level to the main, spherical magic gaps in a given nucleus. However, approximately, for $T \geqslant 1.5$ MeV or so, they can be considered negligible.

With these approximations we have performed the collective-model calculations of the low-lying solutions of the 2D Schrödinger equation with the potential energies calculated using the LSD-C variant of the model. The mass parameter estimate as in Table VII can only be treated as an indication, though much better than just an order-of-magnitude estimate; cf. Ref. [63]. With the potential energies calculated here, it gives the lowest-lying energy eigenvalues for spins close to the critical spins of the order of 1 MeV within a few-hundred-keV margin.

We therefore performed the calculations for three characteristic values of the mass tensor, adjusting the values of $B_{\alpha_{22},\alpha_{22}} = B_{\alpha_{20},\alpha_{20}}$ in such a way that the lowest-energy collective solution for spins close to the transition critical spins corresponds to one of the following three arbitrary choices taken as an estimate of the physically "reasonable" typical values: $E_{\text{coll.}} \approx 0.5$, 1, or 1.5 MeV. With this choice, we cover the possible physical ranges of variations of the wave functions and of the implied quantities such as the most probable deformations and the associated deformation uncertainty intervals which characterize the large-amplitude fluctuations around the equilibrium values.

Using the so-obtained collective wave functions, we are able to calculate the most probable ("dynamic") quadrupole deformations, $(\bar{\alpha}_{20},\bar{\alpha}_{22})_{\text{dyn.}}$, as compared to the static ones, $(\alpha_{20},\alpha_{22})_{\text{stat.}}$, the latter corresponding, by definition, to the minimum on the potential-energy surface. We may select as a measure of the most probable value of a given shape coordinate, say, $\alpha_{\lambda\mu}$, the associated r.m.s. values, $\bar{\alpha}_{\lambda\mu}$, defined by

$$\langle \alpha_{\lambda\mu}^2 \rangle = \int \mathrm{d}\alpha \Psi_n^*(\alpha) \alpha_{\lambda\mu}^2 \Psi_n(\alpha) \rightarrow \bar{\alpha}_{\lambda\mu} = \sqrt{\langle \alpha_{\lambda\mu}^2 \rangle}. \tag{24}$$

In the case of the flat valleys with a nearly constant potential along the bottom and very slowly varying implied collective wave function, the static approximation which consists of attributing the physical sense to the single-point (potential minimum) deformations becomes clearly inappropriate, given the fact that the potential energy changes only a little, whereas the nuclear deformation usually varies considerably. Using the r.m.s. deviations can be considered as the first step towards the estimate of the role of the fluctuations.

An example of the typical behavior of the collective wave-function in the shape-transition range close to the critical transition-spin is given in Fig. 17, for illustration. As can be seen from the figure, the wave function varies relatively slowly along a large deformation stretch ranging from $\alpha_{20} \approx 0.25$ to $\alpha_{20} \approx 1.25$, the variation of the wave-function corresponding to merely about the factor of two; the smaller the inertia, the more spread is the collective wave function.

In Fig. 18, the evolution of the three lowest eigenstates of the collective Hamiltonian is presented for a nucleus representative of the mass range discussed in the article. The lowering of the energy positions is characteristic of the flattening of the surface of the potential energy accompanying the shape transitions. In this illustration of the expected typical behavior we have selected the mass parameters in such a way that the lowest energy corresponds to the 1-MeV level above the minimum of the potential at the transition spin.

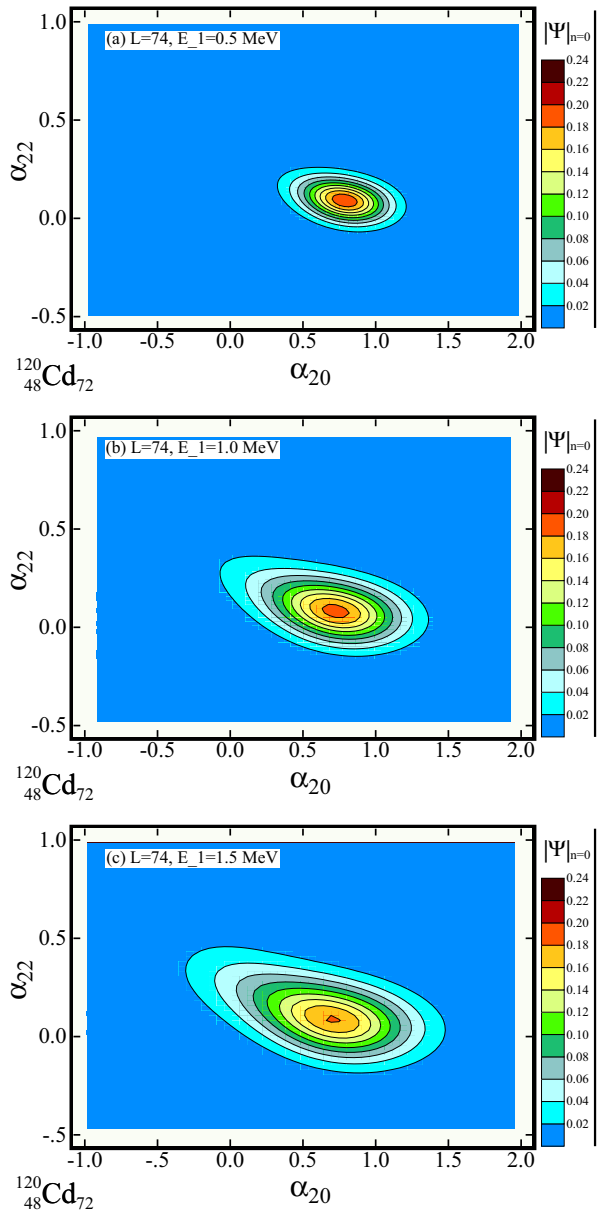

FIG. 17. (Color online) Contour-plot representation of the absolute values of the wave-function solution to the 2D collective Schrödinger equation, Eq. (22), with the constant mass-parameter approximation as discussed in the text. (Top) The energy eigenvalue corresponds approximately to 0.5 MeV above the potential minimum; (middle) approximately 1 MeV above the minimum; (bottom) approximately 1.5 MeV above the minimum. The color scale corresponds to the unit 0.02.

Let us notice that the quantum character of the collective motion implies that each nuclear deformation should be associated with the probability density function $P(\alpha)$ so that the considered probabilities of finding the nucleus in a given "shape interval," $[\alpha - d\alpha, \alpha + d\alpha]$, are given by

$$dP(\alpha) = 2\,|\Psi(\alpha)|^2 d\alpha, \tag{25}$$

where $2\,d\alpha$ denotes the associated volume element in the deformation space. It then follows that the dynamical character

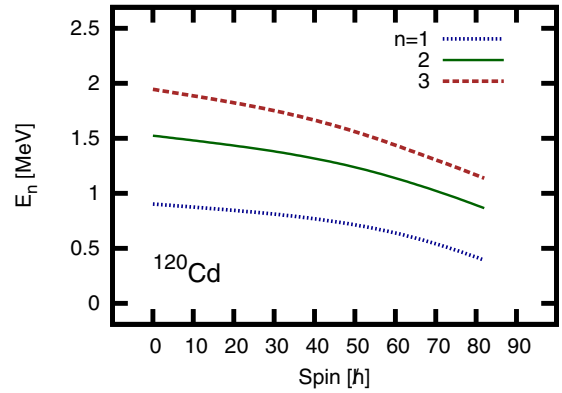

FIG. 18. (Color online) Three lowest-collective-energies solutions of the Schrödinger equation (22) in terms of the variables α_{20} and α_{22}, here presented as functions of spin for ^{120}Cd. The mass parameter is adapted in such a way that the lowest collective energy lies 0.5 MeV above the potential minimum at the critical spin. The symbols $n = 1$, 2, and 3 enumerate the energies of the first three collective solutions, E_1, E_2, and E_3, of Eq. (22).

of the description of the nuclear motion in the shape space can be represented in a compact way, in terms of the expected values of the deformation involved and also by the spreading of the probability distribution described with the help of the dispersion coefficients

$$\sigma_{20} \equiv \sqrt{\langle \alpha_{20}^2 \rangle - \langle \alpha_{20} \rangle^2} \quad \text{and} \quad \sigma_{22} \equiv \sqrt{\langle \alpha_{22}^2 \rangle - \langle \alpha_{22} \rangle^2}. \tag{26}$$

In this fashion one may represent in a compact way the probability distributions associated with the varying flatness of the energy landscapes in terms of four (spin-dependent) quantities: $\bar{\alpha}_{20}$ and σ_{20} as well as $\bar{\alpha}_{22}$ and σ_{22}, cf. Eqs. (24) and (26).

The calculated positions of the quadrupole-axial static deformations and the associated dynamical quantities (circles and squares, respectively) are given in Fig. 19 for the ^{120}Cd nucleus. The differences between the corresponding positions illustrate the impact of the shape-fluctuation effects (dynamical as opposed to static). The figure illustrates at the same time the spreading of the associated probability distribution ("shape uncertainty") with the help of the vertical bars, showing the one-standard-deviation intervals.

The analogous illustration for the triaxial quadrupole deformation and the related motion is presented in Fig. 20 constructed according to the same pattern. Let us observe a much larger spreading in terms of the α_{20} fluctuations expressed in terms of the $\bar{\alpha}_{20}$ deformation together with the associated dispersion, σ_{20}, systematically bigger than σ_{22}; cf. Fig. 20 and compare with Fig. 19 (observe the scale difference on the vertical axes in the two figures). This result underlies the fact that in the case of the Jacobi shape transitions the flattening of the energy landscape in the "direction of elongation" plays a leading role, although the effect of fluctuations in terms of the triaxiality is quite important as well.

Let us also notice that whereas the dispersion σ_{22}, which is a measure of the "uncertainty" in terms the triaxiality parameter α_{22}, reaches its maximum close to the critical spin and then decreases, the dispersion σ_{20} increases nearly monotonically

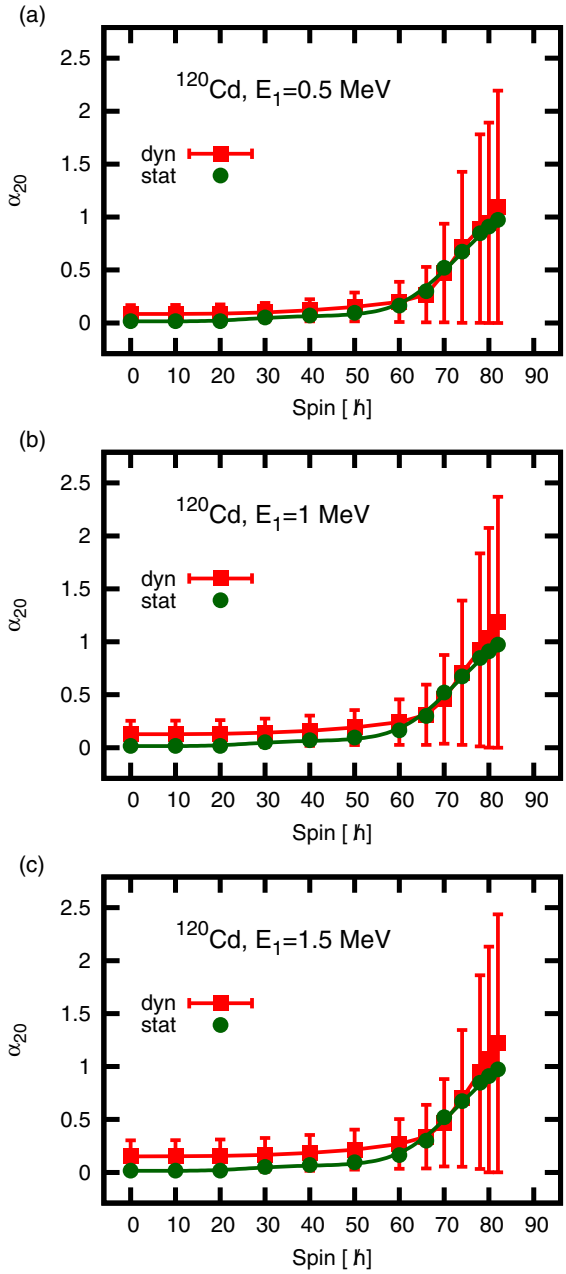

FIG. 19. (Color online) Static values of the axial-symmetry quadrupole deformation α_{20}, circles, taken at the minimum of the total energy landscape and the dynamical most probable quadrupole deformation, $\sqrt{\langle\alpha_{20}^2\rangle}$, squares. The vertical bars give the $\pm\sigma$ deviation intervals around the positions of the centers. The actual values of σ are defined as in Eq. (26). In the present case of the Gaussian-form probability distributions, the deformations contained within the intervals shown represent, approximately, the 68% probability level. The results, from the top to the bottom, correspond to the three choices of the mass parameter as in Fig. 17.

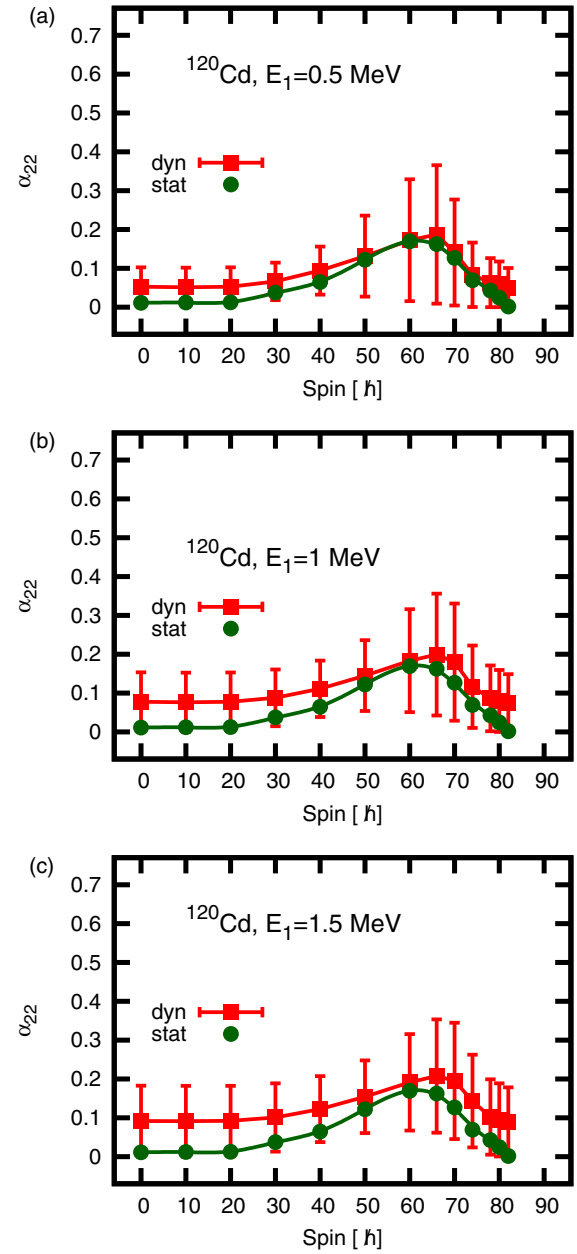

FIG. 20. (Color online) Illustration similar to the one in Fig. 19 but for the nonaxial quadrupole deformation parameter α_{22}. Again the $\pm\sigma$ intervals define the portion of the deformation axis in which the system is to be found with the probability of approximately 68%. (When comparing with the preceding figure, notice the differences in the vertical scale units.)

before the nucleus arrives at the scission. The effect of triaxiality fluctuations may have significant consequences for the future nuclear structure calculations, which will need to take explicitly into account the mechanism of the strong, so-called K mixing in both the rotational-band description in the continuum excitation regime as well as the calculations of the corresponding electromagnetic transition probabilities.

It is instructive to follow the probabilistic consequences of these results. For this purpose, let us combine the traditional elements of the discussion involving a static interpretation and the dynamic (quantum) description followed here. According to the former approach, it is believed that the nucleus fissions from the scission (no return) configuration often referred to as the scission *point*. What is seldom mentioned, however, is the fact that one can talk about a scission *point*, strictly

speaking, only in terms of the *1D* description of the fission process. In the multidimensional spaces we deal with the full hypersurface of the scission configurations.[9] It then follows that the exact scission configuration from which the separation of the two fragments originates is the matter of *probability* with which any of the scission configurations has been reached. Under certain circumstances one may hope that the lowest-energy scission configuration is privileged, as, e.g., at high temperatures where the mass tensor can be considered constant. Generally, however, the mass tensor, depending strongly on the shell effects, may strongly deviate the fission path from the lowest potential-energy scission point(s).

According to the quantum description, we distinguish between two "types" of the associated probability distributions which can be related to

(a) the motion in the 1D deformation subspace along the elongation direction, in our approach principally associated with the α_{20} axis; and
(b) the motion in the orthogonal space, the complementary subspace of the full deformation space, principally determined by the so-called zero-point oscillations.

Suppose that the solution of the Schrödinger equation for the lowest energy is to the leading order proportional to a Gaussian.[10] Let the quadrupole deformation corresponding to the potential minimum be $\alpha_{20}^{\text{min.}}$. Then the probability of finding the nucleus at the scission point, $\alpha_{20}^{\text{scis.}}$—within 1D approach—satisfies approximately

$$P^{\text{sciss.}}\left(\alpha_{20}^{\text{min.}}\right) \propto \exp\left[-\left(\alpha_{20}^{\text{min.}} - \alpha_{20}^{\text{sciss.}}\right)^2 / 2\sigma_{20}^2\right]. \qquad (27)$$

Consequently, the probability of the presence of the system at the scission point under the condition that the energy minimum corresponds to $\alpha_{20}^{\text{min.}}$ depends strongly on the dispersion value σ_{20} as expressed by Eq. (27). However, the full probability of being at any scission configuration will be proportional, additionally, to the factors to an approximation also of the Gaussian structure, depending on the dispersion parameters such as σ_{22} and the similar ones associated with the other deformation degrees of freedom describing the directions orthogonal with respect to that of the elongation axis α_{20}.

To conclude this part of the discussion: It becomes clear that the description of the nuclear shape evolution phenomena—including fission—in the presence of the critical shape changes such as the ones accompanying the Jacobi and Poincaré shape transitions may become more realistic and/or adequate if the solutions of the collective Schrödinger equation are used to calculate the observables of interest. The present section illustrates, we believe in a realistic manner, the expected characteristic impact of the quantum shape fluctuations as well as the differences between the static and dynamic descriptions.

B. The case of Poincaré transitions

All that has been said so far about the Jacobi shape transitions expressed to the leading order with the help of two quadrupole variables, α_{20} and α_{22} simultaneously, can be formulated as well for the Poincaré shape transitions using α_{20} and α_{30} deformations. The latter involve the so-called left-right asymmetry (also referred to as mass asymmetry), i.e., the transition from the inversion-symmetric to the inversion-asymmetric shapes. They can be expressed, to the leading order, by the single multipole α_{30}, the octupole coordinate, often also referred to as "pear-shape" deformation.

A typical illustration of the Poincaré-type shape transition using the $(\alpha_{20},\alpha_{30})$ projection is shown in Fig. 21. Observe the characteristic evolution of the octupole susceptibility which naturally generates the fission-fragment mass asymmetry through the most probable octupole deformations whose expected values increase with spin (see the following figures in this section). This growth is accompanied by a gradual decrease in the fission barrier height.

To calculate the most probable (r.m.s.) α_{30} deformations, the 1D approximation of the potential energies in the direction of α_{30} has been obtained first, through projections on the "octupole valleys" illustrated in Fig. 22. These projections have been used to solve the Schrödinger equation (22), and the corresponding results represent simultaneously the lowest-energy wave function (left scale) and the potential-energy curve (right scale) are illustrated in Fig. 22. Observe a characteristic flattening of the potential energies with increasing spin, eventually evolving into a double-minimum landscape (here plotted for $L = 84\hbar$) symmetric with respect to transformation $\alpha_{30} \to -\alpha_{30}$. Notice a rather tiny barrier between the two minima at spin $L = 84\hbar$, however, with the octupole mass parameter chosen here for the semiquantitative illustration at $B_{30} = 100\hbar^2\ \text{MeV}^{-1}$, sufficient to generate the wave function with a double hump structure.

The forms of the corresponding potential-energy curves translate directly into the characteristic evolution of the related collective wave-functions with increasing spreading (cf. spins

[9]Intuitively, one defines the scission configuration as characterized by the "sufficiently thin average neck radius" so that the two to-be fragments are separated by some very limited area of the diluted nuclear matter only. This condition can be generally satisfied at an infinite number of nuclear shapes, wherefrom the notion of the full hypersurface [an $(n-1)$-dimensional surface in the full space of n dimensions of all the deformation degrees of freedom taken into consideration]. Such a surface can be defined by the condition, e.g., that the average neck radius, say $\overline{R}_{\text{neck}}(\alpha) = R_{\text{limit}}$, the latter "limiting" value defined by the physicist according to some plausible criteria.

[10]Recall that the solutions of the Schrödinger equation with the harmonic-oscillator potential are given by

$$\psi_n(x) = \frac{1}{\sqrt{2^n\, n!\sqrt{\pi}}} \exp(-x^2/2) H_n(x)$$

and for the lowest-energy solution with $n = 0$ we have $H_0(x) = 1$, so that

$$\psi_0^2(y) = \frac{1}{\sqrt{\pi}} \exp(-y^2/2) \text{ with } y \equiv x\sqrt{2}$$

is exactly equal to the probability density function for the normal (Gaussian) distribution with the expected value 0 and standard deviation 1. (The lowest-energy solutions with a potential with a well-defined minimum are often dominated by the ψ_0 element of the harmonic-oscillator basis.)

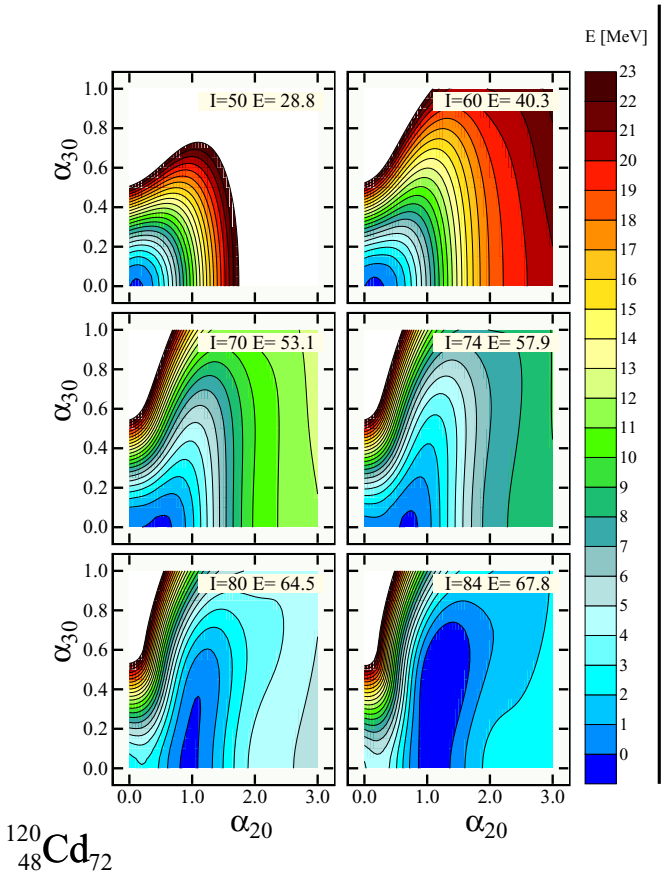

FIG. 21. (Color online) Example of the Poincaré-type shape evolution with spin using the 2D projections (α_{20},α_{30}), analogous to the one in Fig. 16 for the Jacobi-type transition. Two-dimensional projections corresponding to these two figures were obtained using the same full space of collective coordinates over which minimization has been performed. Observe that, strictly speaking, the static Poincaré transition takes place at the very highest spins only, and this close to the fission critical spin (disappearance of the fission barrier). However, the evolution of the dynamic effects with lowering of the octuple valley extending to the "north" is clearly visible.

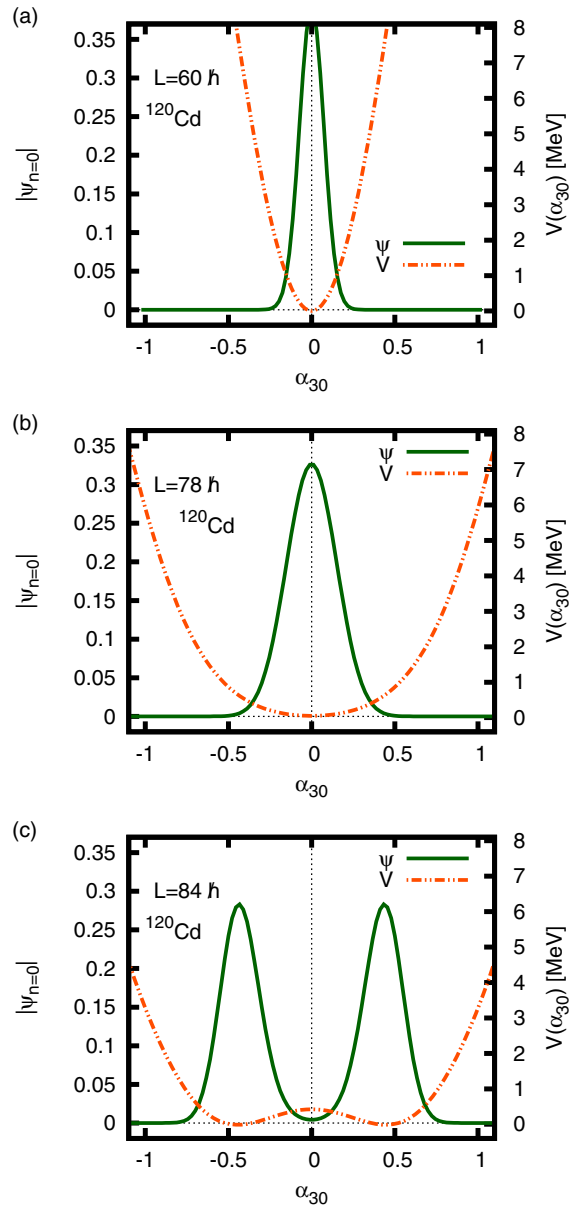

FIG. 22. (Color online) Example of the pear-shape octupole α_{30} evolution with spin. The wave functions (solid lines) correspond to the left-hand side scale, whereas the potentials (dot-dashed lines) correspond to the right-hand scale.

$L = 60$ and $78\hbar$) finishing with the double hump form at the highest spin illustrated.

The characteristic evolution of the pear-shape deformation is illustrated in Fig. 23 as a function of increasing spin in terms of the static and dynamic representations of the shape evolution. Observe that the left-right symmetry breaking obviously takes place in the dynamical description already at the lowest spins. This follows from the fact that at those low spins the zero-phonon collective wave functions have approximately the behavior of a Gaussian, so that at vanishing static equilibrium deformation, $\alpha_{\text{stat.}}$, we necessarily find

$$0 = \alpha^2_{\text{stat.}} < \langle \alpha^2 \rangle_{\text{dyn.}} \sim \int \alpha^2 \exp\left(-\frac{\alpha^2}{\sigma^2}\right) d\alpha \neq 0\,, \qquad (28)$$

which has an immediate impact on the mass asymmetry.

Information presented in Fig. 23 is usually completed with the one showing explicitly the mass asymmetry of the fission fragments translating the r.m.s. deformation parameter α_{30} into the mass asymmetry. To obtain the experiment-comparable fission-fragment mass asymmetry one may, e.g., construct an auxiliary surface composed of two touching ellipsoids and minimize the volume between such an auxiliary object and the actual nuclear surface. The ratio of the volumes of the two ellipsoids makes it possible to obtain an approximate mass ratio of the fission fragments (let us observe that this step of the procedure involves a certain arbitrariness). Of course, alternative ways of extracting the fission-fragment mass asymmetry can be considered; for instance, by integrating directly the volumes of the fragments starting from the point where the nuclear neck can be introduced, the results remain close.

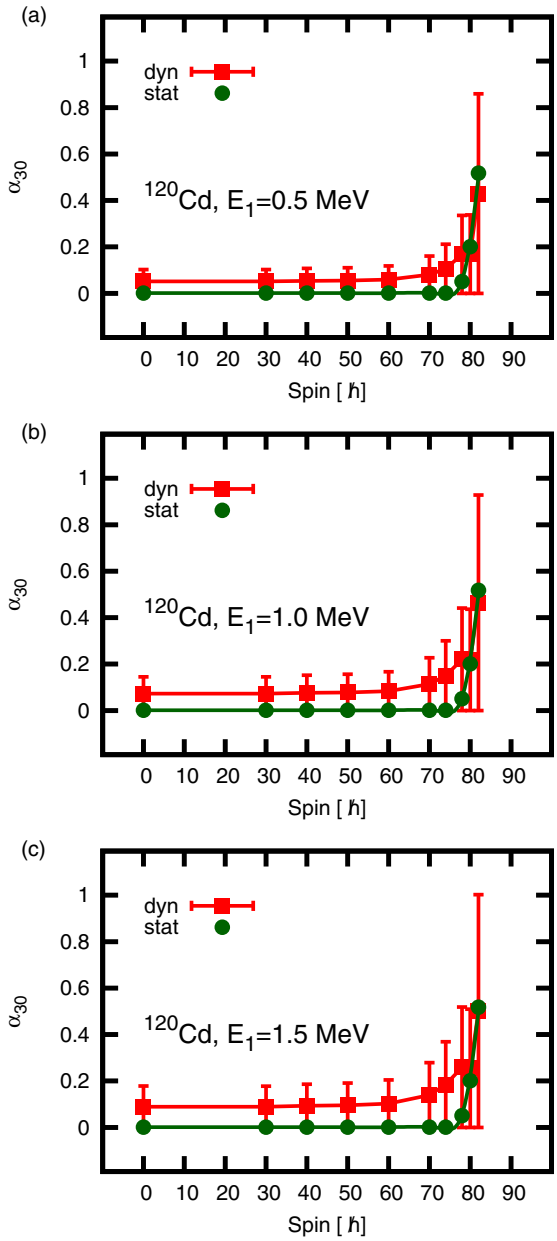

FIG. 23. (Color online) Example of the pear-shape octupole α_{30} evolution with spin, in terms of the static and the dynamic deformations. As before, the static deformations are taken at the equilibrium (minima), whereas the dynamic ones, defined as $\bar{\alpha}_{30}$, are given by relation analogous to the one in Eq. (23).

Combining the information from the two preceding illustrations makes it possible to transform the results of the dynamical deformation estimates directly into the observables: the fission-fragment mass asymmetry as a function of spin. A systematic analysis of the corresponding predictions will be published elsewhere.

Having performed the 1D projection calculations along the pear-shape deformation axis, we proceed to compare the so-obtained results with the analogous ones obtained by solving the 2D Schrödinger equation in the space of $(\alpha_{20} - \alpha_{30})$ variables. In analogy to the definition of the pair of quantities

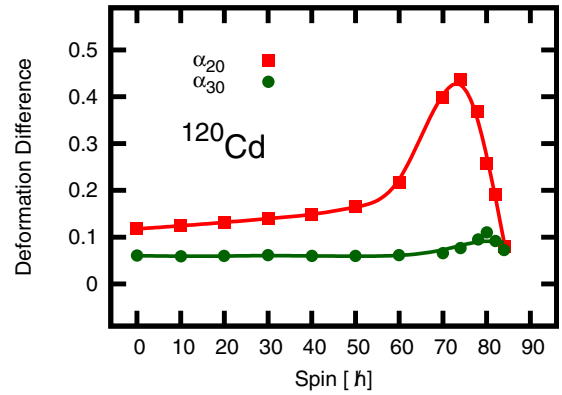

FIG. 24. (Color online) Squares, differences between the dynamical (most likely) quadrupole deformations [in Eq. (24) denoted with the symbol $\bar{\alpha}$] obtained from the solutions of the 2D Schrödinger equation within the space of α_{20} and α_{30} variables *minus* the same quantity calculated from the 2D solutions within the space of α_{20} and α_{22}. Let us emphasize that in the former case, the minimization has been performed, among others, over the α_{22} triaxiality parameter. Positive values of the curve express a "stronger flatness" in the direction of α_{20} with $\alpha_{30} \neq 0$ compared to $\alpha_{22} \neq 0$. Solid dots, differences between the dynamical (most likely) octupole deformations obtained using 2D solutions of the Schrödinger equation in the space of α_{20} and α_{30} deformations and the analogous 1D projection estimates as those in Fig. 23. Observe that the differences are relatively small and nearly constant, suggesting that the 1D approximation offers a good representation of the most probable octupole deformation in the studied case.

in Eq. (26), we introduce the combined dispersion parameters,

$$\sigma_{20} \equiv \sqrt{\langle \alpha_{20}^2 \rangle - \langle \alpha_{20} \rangle^2} \quad \text{and} \quad \sigma_{30} \equiv \sqrt{\langle \alpha_{30}^2 \rangle - \langle \alpha_{30} \rangle^2}, \quad (29)$$

and calculate the resulting estimates using Eq. (24). The potential energies in the case of the 2D solutions using α_{20} and α_{30} were obtained in such a way that at each $\{\alpha_{20},\alpha_{30}\}$, the minimization was performed over α_{22}, as well as the axial-symmetry deformations $\alpha_{\lambda 0}$ for $4 \leqslant \lambda \leqslant 12$.

One of the purposes of this test comparison is to calculate the difference between the predictions related to the octupole motion as obtained using the 1D projections vs the more adequate 2D variant of the problem. We focus on comparing the dynamical (most likely) $\bar{\alpha}_{20}$ and $\bar{\alpha}_{30}$ quadrupole and octupole deformations, respectively [cf. Eq. (24) and Fig. 24], together with the associated dispersion values σ_{20} and σ_{30} of Eq. (29), the latter shown in Fig. 25.

Comparison of the most likely quadrupole and octupole deformations is given in Fig. 24, where, in particular, the differences between the calculations with 2D variant and the 1D projection calculations for the $\bar{\alpha}_{30}$ are shown. Calculations indicate that the 2D description privileges systematically stronger dynamical deformations. These conclusions are strengthened by the results in Fig. 25, where the analogous results for the dispersion parameters are shown.

It will also be instructive to compare the impact of the uncertainties related to the octupole mass parameter $B_{30\,30}$ on the overall behavior of the corresponding wave functions. The corresponding results are presented in Fig. 26 in the form of

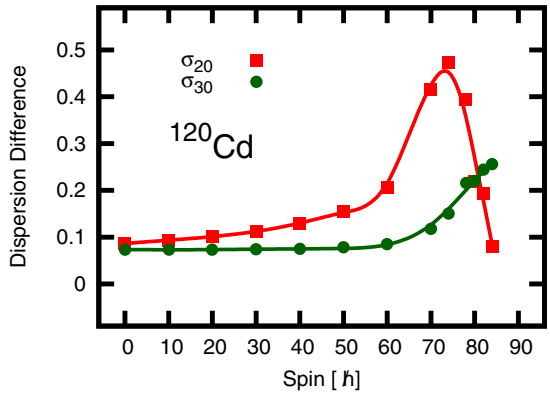

FIG. 25. (Color online) Analogous to the illustration in Fig. 24, but for the differences between the dispersion parameters (cf. the preceding figure).

the contour plots of the ground-state wave functions plotted vs $\alpha_{20} - \alpha_{30}$ coordinates. As could be expected, the lower-energy solution corresponding to the larger mass parameter is peaked more strongly around the potential minimum, whereas the higher-energy solution, with smaller inertia parameters, leads to a more spread distribution. However, the differences can be considered small so that one should not expect significant differences in terms of the results for, e.g., expected values of the deformation parameters and/or associated dispersions (uncertainties). Indeed, the variation range of the $B_{30\,30}$ mass-tensor component which implies the vibrational energy variation ranging from 0.5 to 1.5 MeV can be considered very large. Because the corresponding nuclear energies are expected somewhere within the mentioned broad uncertainty range, the wave functions in Fig. 26 can be seen as a realistic representation and/or approximation of the nuclear collective wave functions.

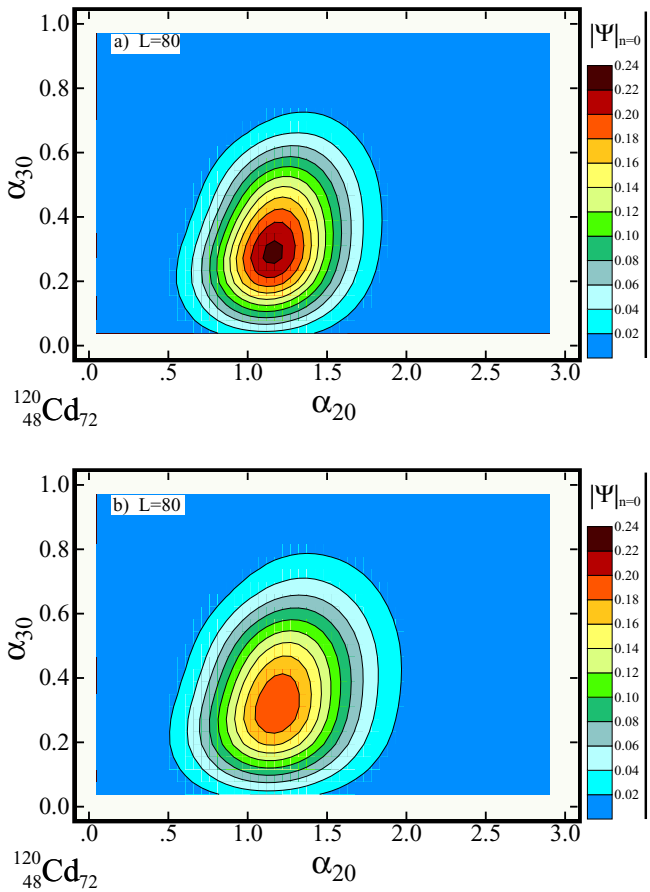

FIG. 26. (Color online) Collective wave-functions solutions of the collective Schrödinger equation [cf. Eqs. (11)–(13)]. (Top) The mass parameter $B_{30\,30}$ has been chosen in such a way that the solution of the 1D projection on the α_{30} axis corresponds to $E_{\text{vib.}} = 0.5$ MeV. (Bottom) Similar to the previous case, but with the $B_{30\,30}$ implying $E_{\text{vib.}} = 1.5$ MeV. For further details, see text.

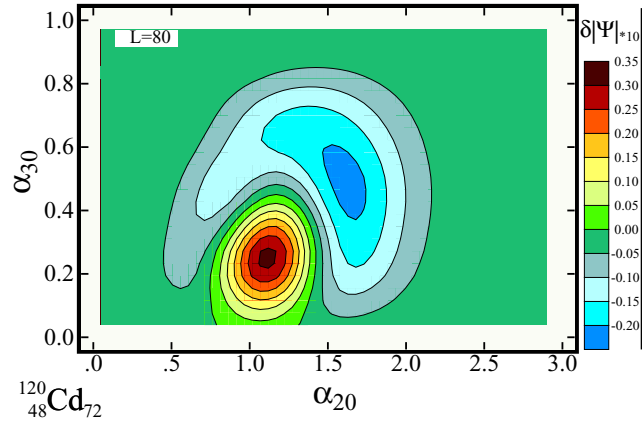

FIG. 27. (Color online) Illustration of the differences between the two wave functions shown in Fig. 26. The one corresponding to the larger value of the mass parameter $B_{30\,30}$ has lower energy *minus* the one corresponding to the smaller value of the discussed mass parameter. Observe that the discussed quantity is very small and, to be able to present the difference, the corresponding difference has been multiplied by the factor of 10.

Because the wave functions corresponding to the two discussed values of the mass parameter $B_{30\,30}$ differ rather little, it may be easier to present the effect by plotting the differences between the two respective wave functions. (Recall that the wave functions of the lowest-energy solutions have a form resembling Gaussians and may be chosen positive so that the sign of the difference describes directly the competition between the two.)

The related difference of the two normalized wave functions (cf. Fig. 27), itself a function of α_{20} and α_{30}, varies between, approximately, -0.02 and $+0.04$. The overall conclusion at this point is that the uncertainties caused by the uncertainties of the (too far an extent unknown) octupole mass parameter at high temperatures are not very large, so that the results presented here for illustration represent rather likely the realistic situations.

IX. SUMMARY AND CONCLUSIONS

In this article we develop a new algorithm based on the macroscopic LSD model. This approach makes it possible to calculate, with an improved precision, the mechanism of the nuclear shape transitions with varying spin in hot rotating

nuclei and the accompanying discussion, in our opinion, offers a more realistic physics insight as compared to previous discussions of the subject.

We focus on two families of the shape transitions known already from the "historical" astrophysics works: The so-called Jacobi and Poincaré shape transitions, Refs. [6,7], respectively. Jacobi transitions lead from axially symmetric nuclear configurations to the triaxially symmetric ones. Poincaré transitions lead from the inversion-symmetric forms to the ones that break the inversion symmetry. Both can be viewed as symmetry-breaking phenomena, but unlike their astrophysical realizations, their nuclear realizations treated by us involve explicitly the description of the quantum critical shape fluctuations. To our knowledge, the Poincaré shape transitions are presented in this context for the first time.

The present article can be seen as a contribution to increasing the performance of the macroscopic-microscopic approaches which combine the powerful nuclear mean-field theory with the approach based on the LDM. Indeed, by focusing on the studies of the nuclear states at high temperature where the quantum shell effects can be neglected we profit from the unique opportunity of optimizing the macroscopic LSD-C model alone, independently of the nuclear mean-field theory aspects. The Jacobi and Poincaré nuclear shape transitions offer valuable experimental test grounds in this context, which are discussed in this article.

To be able to formulate the necessary and sufficient criteria which would allow for an (if possible unambiguous) identification of those transitions in nuclei, one must take into account that both of them may compete when the angular momentum increases. To this end it is important to be able to calculate, in a realistic manner, the probabilities of signals from nuclei which are axially symmetric, triaxial, or left-right asymmetric, and/or which combine these feature when spin increases. Such a competition depends on the large-amplitude fluctuations in terms of both of these modes (Jacobi, Poincaré). We obtain these probabilities approximately by solving numerically the corresponding collective-model Schrödinger equations, to construct the most probable families of shapes from the corresponding collective wave functions.

Taking explicitly into account the presence of either zero-point or large-amplitude motion in the direction of the mass asymmetry coordinate (here α_{30} octupole deformation) introduces the possibility of estimating the fission-fragment mass asymmetry with the help of the quantum, collective-model technique right from the beginning. In particular, the r.m.s. values of the α_{30} deformation can be translated, in a certain model-dependent way, into measurable mass ratios of the fission fragments. This technique reflects in a sensitive manner the octupole-deformation *susceptibility* (e.g., increasing flatness of the nuclear energy landscape without necessarily producing static left-right asymmetric total energy minima) as opposed to the traditional analyses based on the static minima in terms of octupole-type coordinates. (Using this dynamical description also introduces a qualitative difference with respect to estimates of the early Businaro-Gallone approach [64].)

Transitions in question have been traditionally characterized by the critical spin values associated with the static total energy minima: The last spin value at which the preceding symmetry occurs and the first spin value at which the new symmetry arises define the critical spin for the transitions considered. To obtain more realistically these critical-spin values, as well as the description of the fission barriers, we have modified the original LSD model expression of Refs. [25,26] by introducing a deformation-dependent congruence energy term with certain phenomenological parameters whose values have been optimized to the known experimental values of the fission barriers.

This new LSD-C energy expression, with the shape-dependent congruence energy term, lowers the previous discrepancies for the fission barriers for the lighter nuclei considered (^{70,76}Se, ^{75}Br, ^{90,98}Mo) by about 10 MeV, whereas it modifies only slightly the fission barriers for the heavier nuclei for which the agreement has already been good. The remaining discrepancies are of the order of 1 MeV for the mass range between $A \approx 80$ and $A \approx 230$.

The shape-dependent congruence-energy term is expected to imply a better description of the fission barrier heights for increasing spin, as well as for fast-rotating nuclei with the better prospects for the description of the fission cross sections and the shapes of the charge and mass distribution of the fission fragments. The implied additional binding energy lowers also the fission critical spin by $5\hbar - 10\hbar$.

Finally, the stability of the newly obtained LSD-C expression with respect to the basis cutoff, $\lambda_{\max}$ in the nuclear shape parametrization as well as the parametric uncertainties involved by introducing the new parameters to the energy expression have been studied and the results are discussed. The results in this article have been principally limited to a few illustrative cases only. The outcome of more systematic calculations using these methods will be presented elsewhere.

ACKNOWLEDGMENTS

This work has been supported by the COPIN-IN2P3 Polish-French Collaboration under Contract No. 05-119 and the LEA COPIGAL project "Search for the High-rank Symmetries in Subatomic Physics" and the Polish Ministry of Science and Higher Education (Grant No. 2011/03/B/ST2/01894). We would like to thank A. Góźdź and M. Kmiecik for fruitful discussions.

[1] V. M. Strutinsky, Shells in deformed nuclei, Nucl. Phys. A **122**, 1 (1968).

[2] C. Weizsäcker, Zur theorie der Kernmassen, Z. Phys. **96**, 431 (1935).

[3] H. Bethe, Nuclear physics A. Stationary states of nuclei, Rev. Mod. Phys. **8**, 82 (1936).

[4] W. D. Myers and W. J. Swiątecki, Nuclear masses and deformations, Nucl. Phys. A **81**, 1 (1966); also, Anomalies in nuclear masses, Ark. Fys. **36**, 343 (1967).

[5] S. Cohen, F. Plasil, and W. J. Świątecki, Equilibrium configurations of rotating charged or gravitating liquid masses with surface tensor. II, Ann. Phys. **82**, 557 (1974).

[6] C. G. J. Jacobi, *Vorlesungen über Dynamik*, edited by A. Clebsch (G. Reimer, Berlin, 1884).

[7] H. Poincaré, Sur l'équilibre d'une masse fluide animée d'un mouvement de rotation, Acta Math. **7**, 259 (1885).

[8] R. Beringer and W. J. Knox, Liquid-drop nuclear model with high angular momentum, Phys. Rev. **121**, 1195 (1961).

[9] A. J. Sierk, Macroscopic model of rotating nuclei, Phys. Rev. C **33**, 2039 (1986).

[10] D. Ward *et al.*, Search for the Jacobi shape transition in rapidly rotating nuclei, Phys. Rev. C **66**, 024317 (2002).

[11] A. Maj *et al.*, Search for exotic shapes of hot nuclei at critical angular momenta, Nucl. Phys. A **687**, 192 (2001).

[12] A. Maj *et al.*, Evidence for the Jacobi shape transition in hot ^{46}Ti, Nucl. Phys. A **731**, 319 (2004).

[13] M. Kmiecik *et al.*, Strong deformation effects in hot rotating ^{46}Ti, Acta Phys. Pol., B **38**, 1437 (2007).

[14] M. Kmiecik *et al.*, GDR feeding of the highly-deformed band in ^{42}Ca, Acta Phys. Pol., B **36**, 1169 (2005).

[15] M. Ciemała *et al.*, Search for Jacobi shape transition in hot rotating ^{88}Mo nuclei through giant dipole resonance decay, Acta Phys. Pol., B **42**, 633 (2011).

[16] M. Kicińska-Habior *et al.*, Search for a phase transition in the nuclear shape at finite temperature and rapid rotation, Phys. Lett. B **308**, 225 (1993).

[17] D. Pandit *et al.*, Extreme nuclear shapes examined via giant dipole resonance lineshapes in hot light-mass systems, Phys. Rev. C **81**, 061302(R) (2010).

[18] K. Mazurek *et al.*, Effective GDR width of ^{132}Ce at high spins and temperatures from the LSD model, Acta Phys. Pol., B **38**, 1455 (2007).

[19] K. Mazurek, M. Matejska, M. Kmiecik, A. Maj, and J. Dudek, Influence of the level density parameterization on the effective GDR width at high spins, Int. J. Mod. Phys. E **17**, 132 (2008).

[20] B. Herskind *et al.*, Hunting grounds for Jacobi transitions and hyperdeformations, Acta Phys. Pol., B **34**, 2467 (2003).

[21] K. Mazurek, J. Dudek, M. Kmiecik, A. Maj, J. P. Wieleczko, and D. Rouvel, Poincaré shape transitions in hot rotating nuclei, Acta Phys. Pol., B **42**, 471 (2011).

[22] A. Maj, K. Mazurek, J. Dudek, M. Kmiecik, and D. Rouvel, Shape evolution at high spins and temperatures: Nuclear Jacobi and Poincare transitions, Int. J. Mod. Phys. E **19**, 532 (2010).

[23] H. J. Krappe, J. R. Nix, and A. J. Sierk, From heavy-ion elastic scattering to fission: A unified potential for the description of large-scale nuclear collective motion, Phys. Rev. Lett. **42**, 215 (1979); Unified nuclear potential for heavy-ion elastic scattering, fusion, fission, and ground-state masses and deformations, Phys. Rev. C **20**, 992 (1979).

[24] P. Möller and J. R. Nix, Nuclear mass formula with a Yukawa-plus-exponential macroscopic model and a folded-Yukawa single-particle potential, Nucl. Phys. A **361**, 117 (1981); also, Atomic masses and nuclear ground-state deformations calculated with a new macroscopic model, At. Data Nucl. Data Tables **26**, 165 (1981).

[25] K. Pomorski and J. Dudek, Nuclear liquid-drop model and surface-curvature effects, Phys. Rev. C **67**, 044316 (2003).

[26] J. Dudek, K. Pomorski, N. Schunck, and N. Dubray, Hyperdeformed and megadeformed nuclei: Lessons from the slow progress and emerging new strategies, Eur. Phys. J. A **20**, 15 (2004).

[27] K. Pomorski and J. Dudek, Fission barriers within the liquid drop model with the surface-curvature term, Int. J. Mod. Phys. E **13**, 107 (2004).

[28] K. Pomorski, Fission-barrier heights in some newest liquid-drop models, Phys. Scr. T **154**, 014023 (2013).

[29] F. A. Ivanyuk and K. Pomorski, On the Poincaré instability of a rotating liquid drop, Phys. Scr. T **154**, 014021 (2013).

[30] J. Dudek, A. Góźdź, K. Mazurek, and H. Molique, Mean-field theory of nuclear stability and exotic point-group symmetries, J. Phys. G: Nucl. Part. Phys. **37**, 064032 (2010).

[31] K. T. R. Davies and J. R. Nix, Calculation of moments, potentials, and energies for an arbitrarily shaped diffuse-surface nuclear density distribution, Phys. Rev. C **14**, 1977 (1976).

[32] S. Ćwiok, J. Dudek, W. Nazarewicz, J. Skalski, and T. Werner, Single-particle energies, wave functions, quadrupole moments and g-factors in an axially deformed Woods-Saxon potential with applications to the two-centre-type nuclear problems, Comp. Phys. Commun. **46**, 379 (1987).

[33] J. Dobaczewski and J. Dudek, Solution of the Skyrme-Hartree-Fock equations in the Cartesian deformed harmonic oscillator basis I. The method, Comp. Phys. Commun. **102**, 166 (1997).

[34] J. Dobaczewski and J. Dudek, Solution of the Skyrme—Hartree—Fock equations in the Cartesian deformed harmonic oscillator basis II. The program HFODD, Comp. Phys. Commun. **102**, 183 (1997).

[35] W. D. Myers and W. J. Świątecki, The congruence energy: A contribution to nuclear masses, deformation energies and fission barriers, Nucl. Phys. A **612**, 249 (1997).

[36] W. D. Myers and W. J. Świątecki, Nuclear diffuseness as a degree of freedom. II. An improved approach, Phys. Rev. C **60**, 014606 (1999).

[37] P. Möller, J. R. Nix, and W. J. Świątecki, New developments in the calculation of heavy-element fission barriers, Nucl. Phys. A **492**, 349 (1989).

[38] M. Brack, J. Damgaard, A. S. Jensen, H. C. Pauli, V. M. Strutinsky, and C. Y. Wong, Funny hills: The shell-correction approach to nuclear shell effects and its applications to the fission process, Rev. Mod. Phys. **44**, 320 (1972).

[39] S. T. Belyaev, Effect of pairing correlations on nuclear properties, Kgl. Danske Videnskab. Selskab. Matt.-Fys.-Medd. **31**, 1 (1959).

[40] A. Góźdź, K. Pomorski, M. Brack, and E. Werner, The mass parameters for the average mean-field potential, Nucl. Phys. A **442**, 26 (1985).

[41] E. Schrödinger, Quantisierung als Eigenwertproblem (Vierte Mitteilung), Ann. Phys. **81**, 109 (1926).

[42] E. Schrödinger, Quantisierung als Eigenwertproblem (Erste Mitteilung), Ann. Phys. **79**, 361 (1926); cf. Eq. (19).

[43] A. Dobrowolski, A. Góźdź, K. Mazurek, and J. Dudek, Tetrahedral symmetry in nuclei: New predictions based on the collective model, Int. J. Mod. Phys. E **20**, 500 (2011).

[44] L. Próchniak and S. G. Rohoziński, Quadrupole collective states within the Bohr collective Hamiltonian, J. Phys. G **36**, 123101 (2009).

[45] A. Baran, K. Pomorski, A. Łukasiak, and A. Sobiczewski, A dynamic analysis of spontaneous-fission half-lives, Nucl. Phys. A **361**, 83 (1981).

[46] K. Pomorski, Role of the zero-point corrections in fission dynamics, Int. J. Mod. Phys. E **17**, 245 (2008).

[47] J. R. Nix, Further studies in the liquid-drop theory on nuclear fission, Nucl. Phys. A **130**, 241 (1969).
[48] N. Dubray and D. Regnier, Numerical search of discontinuities in self-consistent potential energy surfaces, Comp. Phys. Commun. **183**, 2035 (2012).
[49] W. J. Świątecki, Deformation energy of a charged drop. II. Symmetric saddle point shapes, Phys. Rev. **104**, 993 (1956).
[50] S. Cohen and W. J. Świątecki, The deformation energy of a charged drop: Part V: Results of electronic computer studies, Ann. Phys. (NY) **22**, 406 (1963).
[51] J. R. Nix, The normal modes of oscillation of a uniformly charged drop about its saddle-point shape, Ann. Phys. (NY) **41**, 52 (1967).
[52] S. Trentalange, S. E. Koonin, and A. J. Sierk, Shape parametrization for liquid-drop studies, Phys. Rev. C **22**, 1159 (1980).
[53] J. Dudek, J. Dobaczewski, N. Dubray, A. Góźdź, V. Pangon, and N. Schunck, Nuclei with tetrahedral symmetry, Int. J. Mod. Phys. E **16**, 516 (2007).
[54] A. Góźdź, A. Szulerecka, A. Dobrowolski, and J. Dudek, Symmetries in the intrinsic nuclear frames, Int. J. Mod. Phys. E **20**, 199 (2011).
[55] P. Möller, A. J. Sierk, and A. Iwamoto, Five-dimensional fission-barrier calculations from ^{70}Se to ^{252}Cf, Phys. Rev. Lett. **92**, 072501 (2004).
[56] E. Wigner, On the consequences of the symmetry of the nuclear Hamiltonian on the spectroscopy of nuclei, Phys. Rev. **51**, 106 (1937).
[57] E. Wigner, On the structure of nuclei beyond oxygen, Phys. Rev. **51**, 947 (1937).
[58] W. D. Myers and W. J. Świątecki, Nuclear properties according to the Thomas-Fermi model, Nucl. Phys. A **601**, 141 (1996).
[59] T. S. Fan, K. X. Jing, L. Phair, K. Tso, M. McMahan, K. Hanold, G. J. Wozniak, and L. G. Moretto, Excitation functions and mass asymmetric fission barriers for compound nuclei ^{70,76}Se, Nucl. Phys. A **679**, 121 (2000).
[60] D. N. Delis *et al.*, Mass asymmetric fission barriers for ^{75}Br, Nucl. Phys. A **534**, 403 (1991).
[61] K. X. Jing *et al.*, Transition state rates and mass asymmetric fission barriers of compound nuclei ^{90,94,98}Mo, Nucl. Phys. A **645**, 203 (1999).
[62] L. G. Moretto, S. G. Thompson, J. Routti, and R. C. Gatti, Influence of shells and pairing on the fission probabilities of nuclei below radium, Phys. Lett. B **38**, 471 (1972).
[63] A. Baran and Z. Łojewski, Temperature dependence of mass parameters and fission barriers, Acta Phys. Pol. B **25**, 1231 (1994).
[64] U. L. Businaro and S. Gallone, Asymmetric equilibrium shapes in the liquid drop model, Nuovo Cimento **1**, 629 (1955).